Pergamon

Continental Shelf Research, Vol. 16, No. 7, pp. 875–906, 1996
Copyright © 1996 Elsevier Science Ltd
Printed in Great Britain. All rights reserved
0278–4343/96 $15.00+0.00

0278–4343(95)00028–3

Comprehensive coastal circulation model with application to the Gulf of Maine

DANIEL R. LYNCH,* JUSTIN T. C. IP,*
CHRISTOPHER E. NAIMIE* and FRANCISCO E. WERNER†

(*Received* 3 *October* 1994; *accepted* 4 *January* 1995)

Abstract—A state-of-the-art finite element model is described and applications are shown for the Gulf of Maine. The model is three-dimensional (hydrostatic) with a free surface, fully nonlinear, incorporates advanced turbulence closure and operates in tidal time. Variable horizontal and vertical resolution are facilitated by the use of unstructured meshes. Solutions for the Gulf of Maine illustrate performance in the context of several isolated nonlinear processes. Composite solutions for March–April and July–August time periods are recorded under climatological forcing. The solutions exhibit a general cyclonic central Gulf circulation, a coastal current with several branch points and anticyclonic circulation around Georges Bank. Each of these features is seasonally modulated. The surface circulation is in general agreement with surface drift observations. The circulation at depth shows the combined influence of deep basin topography and baroclinicity.

1. INTRODUCTION

There can be little doubt that coastal circulation will be the focus of intense, interdisciplinary study in the immediate future as we work through the potential impacts of global warming, waste disposal and harvesting pressure on coastal ecosystems. The complex topography typically encountered in such studies begs for a simulation approach on unstructured grids with variable local resolution. The finite element method (FEM) provides just such a capability, backed by a rigorous mathematical framework and supported by a growing software industry providing quality products for generic FEM applications. A basic research goal has been to focus this modeling "technology" on the equations and parameter spaces appropriate to coastal simulation.

Relative to coastal simulation, the finite element "story" has four parts, roughly aligned with the final decades of this century. The story begins in the 1960s, when the method itself achieved astounding success in solid mechanics. During this decade it became clear that complex, three-dimensional vector problems could be solved by large numbers of practicing scientists and engineers worldwide, without the requirement of original repro-

*Dartmouth College, Hanover, New Hampshire, U.S.A.
†University of North Carolina, Chapel Hill, North Carolina, U.S.A.

gramming of the method by each user or for each new study. As these experiences were being consolidated, researchers began to consider use of the FEM in other fields of mathematical physics, including convection/diffusion, fluid mechanics and electricity and magnetism. The decade of the 1970s produced a bloom of interest in fluid mechanics and convection/diffusion in general and in coastal simulation in particular. Developments during this period served to illustrate the potential of the FEM in this area, along with some difficult problems, as new forms of the underlying differential equations posed new challenges which had not been anticipated. By the end of the 1970s, the outlook was mixed, with significant skepticism in some quarters despite some promising successes. It was clear to the FEM community that specific adaptations to the generic FEM approach were likely to be needed in each new physical context. The 1980s was a period of consolidation and analysis, and led to both the sorting out of conceptual/mathematical issues and, later in the decade, to field-scale demonstrations of successful simulation.

It is now apparent that the early skepticism concerning economy, stability and accuracy is no longer appropriate. The FEM is performing well in an important collection of coastal simulation problems, and a firm conceptual foundation explains both success and failure to date. As a result, the FEM is now poised for a decade of progress in a variety of coastal applications, ranging from focused, process-oriented studies to comprehensive simulations of real coastal oceans with real forcing. It is this latter context which provides our working definition of a *comprehensive model*:

> A *comprehensive model* is one which provides shelf-scale geographic coverage; adequate local resolution of topography, coast and flow features; and internal physics sufficient to capture all important shelf processes in tidal time.

Herein we first review the historical progress alluded to above in greater detail. We then summarize a basic implementation of a full-featured three-dimensional shelf model which incorporates advanced turbulence closure. A case study in the Gulf of Maine illustrates model performance relative to several important nonlinear shelf processes. Implied by the examples is the successful realization of a comprehensive FEM circulation model.

2. REVIEW

Oceanographic studies employing the FEM have been appearing since the early 1970s, inspired by the spectacular worldwide success in solid mechanics and diffusion problems. From the start, the primary attraction of the FEM has been the rigorous mathematical approach to problems with strong spatial inhomogeneity, arising either from topography (banks, coast) or from steep internal gradients in the flow field (e.g. fronts, jets, etc.). The use of unstructured, nonuniform computational grids (i.e. with no *a priori* orientations or connections) of variable size triangular elements allows, in principle, high resolution of such local features without necessarily sacrificing the horizontal extent of the model. The Galerkin method in conjunction with such meshes provides natural and rigorous integration of local and far-field interactions. Following two decades of intensive development and application to the general circulation (Fix, 1975; Haidvogel *et al.*, 1980; Le Provost, 1986; Bernier, 1990; Ma, 1993; Iskandarani *et al.*, 1995; LeProvost *et al.*, 1994; Myers and Weaver, 1995), to the shelf break (Werner, 1987), to oceanic tides (Platzman, 1978; Le Provost and Vincent, 1986; Vincent and Le Provost, 1988; Le Provost *et al.*, 1991; Canceill *et al.*, 1994; LeProvost *et al.*, 1995) and to continental shelf studies (below), the benefits of

the FEM for oceanographic applications are now firmly established and workable algorithms are available.

Studies of estuarine and shelf circulation appeared as early as 1973 (Grotkop, 1973; Wang and Connor, 1975), and the early (pre-1976) experiences with the two-dimensional shallow water equations are summarized in Pinder and Gray (1977). These experiences with time-stepping methods demonstrated clearly the potential of the method, as well as several persistent difficulties including unexplained instabilities, computational parasites and high computational cost—typical symptoms for any new application area.

In the late 1970s, investigators at several institutions were considering the harmonic or frequency domain formulation of the two-dimensional shallow water problem: Pearson and Winter (1977) and Jarmart (1980) at the University of Washington; Le Provost and Poncet (1978) at the Institut de Mecanique, Grenoble; Platzman (1978) at the University of Chicago; and Lynch and Gray (1979) at Princeton University. Each team arrived more or less concurrently at the same finding: that the natural reformulation of the problem in terms of a higher-order, Helmholtz-type operator produced excellent results even with the simplest of finite elements (linear triangles). The Princeton team also developed highly effective time-stepping methods based on the analogous rearrangement of the primitive equations in the time domain to obtain the shallow water wave equation; derived their stability limits; and demonstrated the equivalence between time-stepping and frequency-domain solutions. The remarkable feature of the "wave equation"-based algorithms is the simultaneous solution of the "computational parasite" problem with the introduction of important computational efficiencies previously associated only with finite difference methods: explicit time-stepping methods with no required matrix factorization; and semi-implicit time-stepping methods requiring factorization of only the matrix for the free surface elevations. A review of this early work appears in Lynch (1983). Subsequent work by Walters and Carey (1984) and Kinnmark and Gray (1984) extended the formal analysis of wave equation methods, confirming in greater generality the initial findings. Foreman (1983) developed favorable comparisons between the wave equation implementation on linear elements and finite difference schemes in common use.

Several field-scale investigations using wave equation methods followed. In 1984, an informal working group of FEM modelers—the "tidal flow forum" (TFF)—formed to develop a public-domain data set for the English Channel and the southern bight of the North Sea. Eleven modeling studies have appeared; seven of these use the finite element method [see the special issues of *Advances in Water Research*, September 1987, September 1989 and December 1989; and the reviews by Werner and Lynch (1988) and Werner (1995)]. Among the specific conclusions which have been drawn are:

(1) three different FEM models based in wave equation formulations (explicit, implicit and harmonic) agree with each other and with the data (Werner and Lynch, 1987; Gray *et al.*, 1987; Walters, 1987);
(2) the FEM properly represents several important nonlinear interactions and has led to the isolation of key weaknesses in the TFF data base (Werner and Lynch, 1989; Walters and Werner, 1989);
(3) within the limits of the TFF exercise, the FEM has reached a level of development equivalent to established finite difference methods (Praagman *et al.*, 1989; Jamart and Ozer, 1989).

Additional recent field-scale FEM studies have been carried out in the Gulf of

Venezuela/Lake Maracaibo (Lynch *et al.*, 1990); the Alborán Sea (Lynch *et al.*, 1989); the Gulf of Maine (Lynch *et al.*, 1992); the Bight of Abaco (Westerink *et al.*, 1989); the southwest coast of Vancouver Island (Foreman and Walters, 1990; Foreman, 1991; Foreman *et al.*, 1992a, b; Walters and Foreman, 1992; Foreman *et al.*, 1993); the South Atlantic Bight (Werner *et al.*, 1993a); the Delaware Bay (Walters, 1992); the Gulf of Mexico (Westerink, 1990; Westerink *et al.*, 1992; Blain *et al.*, 1994); and the Atlantic Ocean basin (Genco, 1993). Several of these studies are active today, and have been extended to include three-dimensional computations based on conventional velocity (Lynch and Werner, 1991b) and novel "direct stress" approaches (Luettich and Westerink, 1991; Luettich *et al.*, 1994); studies of convergence of solutions based on mesh discretization (Westerink *et al.*, 1994; Luettich and Westerink, 1995; Lynch *et al.*, 1995); radiation boundary conditions (Johnsen and Lynch, 1994, 1995); and computations on special coordinate systems (Kolar *et al.*, 1994a). Concurrent with this intense quickening of "wave equation" FEM activity, a FEM mesh generator has been developed by the Canadian Department of Fisheries and Oceans (Henry, 1988; Henry and Walters, 1993). This package operates on standard bathymetric data sets and creates graded meshes with uniform Courant number.

Of direct concern here is the family of three-dimensional wave equation FEM models recently constructed by Lynch and Werner (1987; 1991a) and Lynch *et al.* (1992). Included is a linearized harmonic (including steady-state) model and a nonlinear time-stepping model. Testing to date includes tidal, wind-drive and diagnostic baroclinic computations employing simplified turbulence closure. Applications have been made to several of the field-scale studies described above, and to the Gulf of Maine/Georges Bank (reviewed below). The Gulf of Maine work includes nonlinear interactions by iteration with the linearized harmonic model and stratification-dependent closure.

The desirability of a full-featured finite element model for coastal circulation is apparent. Herein we implement such a model by adding prognostic density evolution and advanced turbulence closure to the basic three-dimensional time-domain framework of Lynch and Werner (1991a). The Mellor–Yamada (1982) level 2.5 closure is employed, with important adjustments by Galperin *et al.* (1988) and Blumberg *et al.* (1992). The resulting model represents a synthesis of over two decades of progress in both finite element and finite difference research.

3. PROGNOSTIC TIME-DOMAIN MODEL

We introduce here a nonlinear time-domain model following the algorithmic approach of Lynch and Werner (1991a), with improvements and extensions. It is a free-surface, tide-resolving model based on the conventional three-dimensional shallow water equations, with the depth-averaged continuity equation expressed in "wave equation" form. The Galerkin weighted residual method is used to obtain the weak form, which is discretized on simple linear elements (triangular in the horizontal, linear in the vertical) with all variables expressed in the same linear basis. A general terrain-following vertical coordinate is used, with a flexible FEM approach to vertical resolution. This provides continuous tracking of the free surface and proper resolution of surface and bottom boundary layers. Temperature and/or salinity are transported in tidal time and the density field is closed prognostically via an equation of state.

Vertical mixing of momentum, heat and mass is represented by a level 2.5 turbulence closure scheme (Mellor and Yamada, 1982). This approach provides stratification- and

shear-dependent mixing coefficients which evolve with the simulation and requires the prognostic evaluation of two additional macroscopic state variables to characterize the turbulence distribution. The improvements of Galperin *et al.* (1988) have been found to be very important in avoiding unphysical situations on Georges Bank and have been adopted as standard. In the horizontal, Smagorinsky-type closure provides shear- and mesh scale-dependent eddy viscosity (Smagorinsky, 1963).

3.1. *Governing equations*

We solve the three-dimensional hydrodynamic equations with the conventional Boussinesq and hydrostatic assumptions. The subgrid-scale dissipation is represented in eddy viscosity (diffusivity) form, parameterized in terms of stratification plus turbulent kinetic energy and mixing length, both of which evolve at the macroscale. The following notation is used:

$\mathbf{v}(x,y,z,t)$ is the fluid velocity, with Cartesian components (u,v,w)
$\bar{\mathbf{v}}(x,y,t)$ is the vertical average of $\mathbf{v}$
$\zeta(x,y,t)$ is the free surface elevation
$h(x,y)$ is the bathymetric depth
$H(x,y,t)$ is the total fluid depth, $H = h + \zeta$
$\rho(x,y,z,t)$ is the fluid density; ρ_0 is a reference value
$T(x,y,z,t)$ is the fluid temperature
$S(x,y,z,t)$ is the fluid salinity
$q^2(x,y,z,t)/2$ is the turbulent kinetic energy
$l(x,y,z,t)$ is the turbulent mixing length
$N_m(x,y,z,t)$ is the vertical eddy viscosity
$N_h(x,y,z,t)$ is the vertical eddy diffusivity for heat and salt
$N_q(x,y,z,t)$ is the vertical eddy diffusivity for q^2 and $q^2 l$
$\mathbf{F}_m, F_T, F_S$ are non-advective horizontal exchanges of momentum, heat, and salt
$\mathbf{g}$ is gravity
$\mathbf{f}$ is the Coriolis vector, directed vertically with magnitude f
∇ is the gradient operator; ∇_{xy} is its horizontal part
$\frac{\mathrm{d}}{\mathrm{d}t}$ is the material derivative, $\frac{\mathrm{d}}{\mathrm{d}t} = \frac{\partial}{\partial t} + \mathbf{v} \cdot \nabla$
(x,y) are the horizontal Cartesian coordinates
z is the vertical coordinate, positive upward; $-h \leqslant z \leqslant \zeta$
t is time.

There are six canonical three-dimensional state variables for which conventional transport equations are written. We have the two horizontal components of the momentum equation:

$$\frac{\mathrm{d}\mathbf{v}}{\mathrm{d}t} + \mathbf{f} \times \mathbf{v} + g\nabla_{xy}\zeta - \frac{\partial}{\partial z}\left(N_m \frac{\partial \mathbf{v}}{\partial z}\right) = -\frac{\mathbf{g}}{\rho_0}\int_z^{\zeta} \nabla_{xy}\rho \mathrm{d}z + \mathbf{F}_m \tag{1}$$

heat and salt conservation:

$$\frac{\mathrm{d}T}{\mathrm{d}t} - \frac{\partial}{\partial z}\left(N_h \frac{\partial T}{\partial z}\right) = F_T \tag{2}$$

Table 1. *Summary of constants associated with the vertical closure. Column* I *contains the Mellor–Yamada* (1982) *experimental constants, plus* E_3 *from Blumberg* et al. (1992) *and von Karman's constant* κ. *Column* II *contains the formulae from Galperin* et al. (1988) *used in equations* (9) *herein. Their numerical values appear in Column* III.

I	II	III
$A_1 = 0.92$	$g_0 \equiv 1.0 - 6A_1/B_1$	$g_0 = 0.66747$
$A_2 = 0.74$	$g_1 \equiv 6A_1 + B_2$	$g_1 = 15.620$
$B_1 = 16.6$	$g_2 \equiv A_1(g_0 - 3C_1)$	$g_2 = 0.39327$
$B_2 = 10.1$	$g_3 \equiv 3A_1A_2[(B_2 - 3A_2)g_0 - 3C_1g_1]$	$g_3 = 3.0858$
$C_1 = 0.08$	$g_4 \equiv 3A_2g_1$	$g_4 = 34.676$
$E_1 = 1.8$	$g_5 \equiv 9A_1A_2$	$g_5 = 6.1272$
$E_2 = 1.33$	$g_6 \equiv A_2g_0$	$g_6 = 0.49393$
$E_3 = 0.25$		
$\kappa = 0.4$		

$$\frac{\mathrm{d}S}{\mathrm{d}t} - \frac{\partial}{\partial z}\left(N_h \frac{\partial S}{\partial z}\right) = F_S \tag{3}$$

and and equations for the turbulent kinetic energy and mixing length:

$$\frac{\mathrm{d}q^2}{\mathrm{d}t} - \frac{\partial}{\partial z}\left(N_q \frac{\partial q^2}{\partial z}\right) = 2\left[N_m\left(\left(\frac{\partial u}{\partial z}\right)^2 + \left(\frac{\partial v}{\partial z}\right)^2\right) + \frac{g}{\rho_0} N_h \frac{\partial \rho}{\partial z}\right] - 2\left[\frac{q^3}{B_1 l}\right] \tag{4}$$

$$\frac{\mathrm{d}q^2 l}{\mathrm{d}t} - \frac{\partial}{\partial z}\left(N_q \frac{\partial q^2 l}{\partial z}\right) = lE_1\left[N_m\left(\left(\frac{\partial u}{\partial z}\right)^2 + \left(\frac{\partial v}{\partial z}\right)^2\right) + \frac{g}{\rho_0} N_h \frac{\partial \rho}{\partial z}\right] - lW\left[\frac{q^3}{B_1 l}\right] \tag{5}$$

wherein E_1 and B_1 are experimental constants (Mellor and Yamada, 1982) and W is a wall proximity function (Blumberg *et al.*, 1992) (Table 1). The final state variable is the free surface $\zeta(x,y,t)$ whose evolution is defined by the vertically integrated continuity equation

$$\frac{\partial \zeta}{\partial t} + \nabla_{xy} \cdot \int_{-h}^{\zeta} \mathbf{v}\,\mathrm{d}z = 0 \tag{6}$$

The system is closed with several equilibrium relations. The three-dimensional continuity equation provides a means for computing vertical velocity w in terms of the horizontal velocity:

$$\frac{\partial w}{\partial z} = \nabla_{xy} \cdot \mathbf{v} \tag{7}$$

The density is related to temperature and salinity by the equation of state (Gill, 1982):

$$\rho = \rho(T,S) \tag{8}$$

evaluated at constant pressure. The closure for the vertical turbulent mixing coefficients is

$$N_m = qls_m \tag{9a}$$

$$N_h = qls_h \tag{9b}$$

$$N_q = qls_q \tag{9c}$$

where s_q is a constant and the stability functions s_m and s_h are simple algebraic functions of the local stratification

$$G_h \equiv \frac{l^2}{q^2}\frac{g}{\rho_0}\frac{\partial \rho}{\partial z}$$

(Galperin *et al.*, 1988):

$$s_m = \frac{(g_2 - g_3 G_h)}{(1. - g_4 G_h)(1. - g_5 G_h)} \tag{9d}$$

$$s_h = \frac{g_6}{(1. - g_4 G_h)} \tag{9e}$$

$$s_q = 0.2 \tag{9f}$$

The constants g_i, introduced here for simplicity, are related in Table 1 to the standard constants of Mellor and Yamada (1982) derived from experiment. Also from Galperin *et al.* (1988) we enforce an upper bound on the mixing length under stable stratification:

$$l \leqslant \frac{0.53q}{\sqrt{-\frac{g}{\rho_0}\frac{\partial \rho}{\partial z}}} \tag{10}$$

This implies an effective lower limit $G_h \geqslant -0.28$. Under unstable stratification, G_h is capped at the upper limit $G_h \leqslant 0.0233$. Among other things, this prevents the computation of negative diffusivity according to (9d) and (9e). Finally, the non-advective horizontal exchanges $\mathbf{F}_m$, F_T, etc. are all expressed in Laplacian forms, e.g.

$$\mathbf{F}_m = \nabla_{xy} \cdot (A \nabla_{xy} \mathbf{v}) \tag{11}$$

with A given in terms of the local shear and grid scale δ as in Smagorinsky (1963):

$$A = 0.28\delta^2 \sqrt{\left(\frac{\partial \bar{u}}{\partial x} - \frac{\partial \bar{v}}{\partial y}\right)^2 + \left(\frac{\partial \bar{v}}{\partial x} + \frac{\partial \bar{u}}{\partial y}\right)^2} \tag{12}$$

3.2. *Boundary conditions*

We solve these equations subject to conventional horizontal boundary conditions as described in previous studies. Vertical boundary conditions are posed as follows. For the horizontal velocity, the atmospheric shear stress is specified at the surface

$$N_m \frac{\partial \mathbf{v}}{\partial z}\bigg|_{z=\zeta} = H\boldsymbol{\Psi} \tag{13a}$$

At the bottom we use a conventional quadratic slip condition relating shear stress to the bottom velocity $\mathbf{v}_b$ via the dimensionless quadratic bottom stress drag coefficient, C_d

$$N_m \frac{\partial \mathbf{v}}{\partial z}\bigg|_{z=-h} = C_d \,|\, \mathbf{v}_b \,|\, \mathbf{v}_b \tag{13b}$$

Atmospheric heat input is specified at the surface as a "Type III" or radiation condition with heating rate α and equilibrium temperature T_0:

$$N_h \frac{\partial T}{\partial z}\bigg|_{z=\zeta} = -\alpha(T - T_0) \tag{14a}$$

At the bottom, heat flux is assumed negligible

$$N_h \frac{\partial T}{\partial z}\bigg|_{z=-h} = 0. \tag{14b}$$

Analogous no-flux conditions are imposed on S at surface and bottom. For q^2, Dirichlet conditions are enforced at surface and bottom:

$$q^2 = B_1^{2/3} u_*^2 \tag{15}$$

with the friction velocity

$$u_*^2 = \left| N_m \frac{\partial \mathbf{v}}{\partial z} \right|$$

specified as in the velocity boundary conditions. Consistent with the slip condition at the bottom, the computational bottom $z_b = -h$ is located within the constant stress layer at a height $\xi_b = 1$ m above the actual sea floor. The mixing length at the computational bottom is set in accord with the law of the wall:

$$l = \kappa \xi_b \tag{16}$$

where $\kappa = 0.4$ is von Karman's constant. At the free surface, the mixing length is conventionally set to zero, although we find this unsatisfying in some situations. For generality we enforce the equivalent of (16) at a distance ξ_s from the free surface. The wall proximity function W is taken from Blumberg *et al.* (1992) and incorporates asymmetry among surface and bottom "walls":

$$W = 1 + E_2\left[\frac{l}{\kappa(z - z_b + \xi_b)}\right]^2 + E_3\left[\frac{l}{\kappa(\zeta - z + \xi_s)}\right]^2 \tag{17}$$

with $l/\kappa d$ approaching unity as the distance d from either wall vanishes. Finally, kinematic conditions are enforced on the vertical velocity w at the surface,

$$w = \frac{\partial \zeta}{\partial t} + \mathbf{v} \cdot \nabla_{xy} \zeta \tag{18a}$$

and at the bottom,

$$w = -\mathbf{v} \cdot \nabla_{xy} h \tag{18b}$$

Both are enforced as Dirichlet conditions on the z-derivative of (7), as in Lynch and Naimie (1993).

3.3. *Wave continuity equation*

For sea surface elevation ζ, we rearrange (6) and the vertically integrated momentum equations to obtain the shallow water wave equation as in Lynch and Werner (1991a):

$$\frac{\partial^2\zeta}{\partial t^2} + \tau_0\frac{\partial\zeta}{\partial t} - \nabla_{xy}\cdot\left[-\mathbf{v}\,|_{z=\zeta}\frac{\partial\zeta}{\partial t} + \int_{-h}^{\zeta}\left[\mathbf{v}\cdot\nabla\mathbf{v} + \frac{g}{\rho_0}\int_z^{\zeta}\nabla_{xy}\rho\mathrm{d}z' - \mathbf{F}_m\right]\mathrm{d}z\right.$$
$$\left. + gH\nabla_{xy}\zeta + \mathbf{f}\times H\overline{\mathbf{v}} - \tau_0 H\overline{\mathbf{v}} - N_m\frac{\partial\mathbf{v}}{\partial z}\bigg|_{z=\zeta} + N_m\frac{\partial\mathbf{v}}{\partial z}\bigg|_{z=-h}\right] = 0 \tag{19}$$

where τ_0 is a numerical constant (Kinnmark, 1986). Inserting the boundary conditions (13) into (19), we arrive at the final form of the wave equation:

$$\frac{\partial^2\zeta}{\partial t^2} + \tau_0\frac{\partial\zeta}{\partial t} - \nabla_{xy}\cdot\left[-\mathbf{v}\,|_{z=\zeta}\frac{\partial\zeta}{\partial t} + \int_{-h}^{\zeta}\left[\mathbf{v}\cdot\nabla\mathbf{v} + \frac{g}{\rho_0}\int_z^{\zeta}\nabla_{xy}\rho\mathrm{d}z' - \mathbf{F}_m\right]\mathrm{d}z\right.$$
$$\left. + gH\nabla_{xy}\zeta + \mathbf{f}\times H\overline{\mathbf{v}} - \tau_0 H\overline{\mathbf{v}} - H\boldsymbol{\Psi} + C_d|\mathbf{v}_b|\,\mathbf{v}_b\right] = 0 \tag{20}$$

We solve (20) for ζ instead of the primitive equation (6) in order to preserve established gravity-wave performance on simple elements (Lynch and Gray, 1979). The only departure here from the three-dimensional wave equation in Lynch and Werner (1991a) is the detailed form of the convective terms, which is similar to the two-dimensional form used by Luettich *et al.* (1992) and Kolar *et al.* (1994b). In three dimensions, we use the identity

$$\frac{\partial}{\partial t}\int_{-h}^{\zeta}\mathbf{v}\mathrm{d}z \equiv \mathbf{v}|_{z=\zeta}\frac{\partial\zeta}{\partial t} + \int_{-h}^{\zeta}\frac{\partial\mathbf{v}}{\partial t}\mathrm{d}z \tag{21}$$

in conjunction with the momentum equation, *en route* to equations (19) and (20).

3.4. *Vertical meshing*

The vertical mesh is adjusted in tidal time to track the free surface. Interior node deployment is arbitrary and may be selected on case-specific criteria. The time-dependent mesh deformation is accounted for as in Lynch and Werner (1991a). In several of the runs reported here, we use a smoothly graded mesh obtained with the transformation

$$z(\varepsilon) = -h + \varepsilon(h + \zeta) - \beta\sin(2\pi\varepsilon) \tag{22}$$

wherein ε increases linearly with node number, from 0 at bottom to 1 at the free surface. The constant β is set to give the desired boundary layer resolution. Recall that the bottommost node, $z = z_b = -h$, lies $\xi_b = 1$ m above the true bottom. We find, as a rule of thumb, that good representation of the bottom boundary layer is obtained with the bottom element approximately the same size as ξ_b (Naimie, 1995).

3.5. *Baroclinic pressure gradient*

The baroclinic pressure gradient is computed utilizing level surfaces as in Naimie *et al.* (1994). The density is interpolated from the FEM vertical grid onto level triangular grids at fixed depths (10 m spacing from surface to 60 m; 15 m spacing to 75 m; 25 m spacing to 250 m; 50 m spacing to 500 m; and 100 m below). $\nabla_{xy}\rho$ is computed on these surfaces and interpolated back to the original vertical grid, where the appropriate vertical integrations are performed.

3.6. *Solution procedure*

The method of solution for ζ and the horizontal velocity is essentially unchanged from Lynch and Werner (1991a). It is based on the Galerkin weak-form of the governing

equations, with nodal quadrature for evaluation of the inner products. A semi-implicit time-stepping procedure is used to solve the implicit wave equation for elevation. This involves three time-levels with implicit, centered gravity waves and centered explicit nonlinearities. The essential computational act is the solution of a sparse, symmetric, positive-definite two-dimensional FEM matrix which is time-invariant. This is followed by a two time-level solution for velocity with rotation, barotropic pressure, vertical shear and bottom stress terms centered and implicit in time and all other terms lagged and explicit. The use of nodal quadrature reduces this calculation to a simple tridiagonal matrix inversion. The vertical variation of viscosity (and diffusivities) is represented by element-wise constants which are recomputed at the beginning of each time step and held fixed during the time step.

The discretization and solution of the T, S, q^2 and q^2l equations are analogous to that for velocity. The decay terms in the q^2 and q^2l equations are treated in each time step as quasi-linear, first-order decays and handled implicitly, along with vertical diffusion in general, to avoid stability constraints. These variables therefore require only tridiagonal matrix solution in each time step, like the horizontal velocity.

The vertical velocity is obtained as in Lynch and Naimie (1993) from the z-derivative of the continuity equation. With nodal quadrature, this calculation is also tridiagonal. Finally, the mesh is adjusted in every time step to track the movement of the free surface and distribute it among the nodes at depth according to, e.g., equation (22).

4. THE GULF OF MAINE

The Gulf of Maine is a semi-enclosed coastal sea on the north-west Atlantic Shelf, comprising three primary deep basins which exceed 200 m depth. The Gulf is bounded at its seaward end by Georges Bank, Nantucket Shoals and Browns Bank, which are roughly defined by the 60 m isobath. Three primary channels connect the Gulf with adjacent waters: Northeast Channel, with sill depth at approximately 230 m; Great South Channel, sill depth 70 m; and "Northern Channel" (north of Browns Bank), approximately 140 m deep [see Fig. 1(a)].

The basic Gulf-wide circulation is depicted in Fig. 1(b)—a composite schematic summarizing numerous observational, theoretical and modeling studies, beginning with the seminal work of Bigelow (1927). Generally, most important shelf processes are operative in the Gulf and contribute in various blends to the features shown. These include two primary and distinct inflows through Northern Channel (Scotian Shelf water) and Northeast Channel (slope water); deep-water formation in the three major Gulf basins; tides, tidal mixing and tidal rectification; wind; stratification and frontal circulation; freshwater inflow along the coast; and local estuarine processes. These processes are all inextricably interwoven at various length- and time-scales. Therefore, any comprehensive modeling strategy must ultimately be capable of nonlinear, simultaneous simulation of all of them.

The resolution demands could be overwhelming in this context. As a starting point, the internal radius of deformation sets an upper limit on mesh size at 5–10 km. However, tidal rectification and frontal circulation can demand resolution of order 2 km, while properly equilibrated inflows from the Scotian Shelf demand upstream spatial coverage of order four shelf widths, i.e. horizontal coverage of order 1000 km. Similarly in the vertical, proper resolution of surface and bottom heat and momentum transfers demands vertical

resolution of order 1 m, with total depth reaching 300 m in the Gulf basins and 1000 m or more at the shelf break. Uniform gridding over these ranges produces an estimated 250,000 horizontal cells, with perhaps on average 200 vertical cells. Coupling these spatial needs with the requirements of simulating nonlinear dynamics in tidal time would produce a formidable computational burden.

By contrast, the FEM mesh depicted in Fig. 2 includes 6756 horizontal nodes and 12,877 triangles. Coverage extends from the Laurentian Channel to the western tip of Long Island, and seaward to roughly the 1000 m isobath, beyond which it terminates in a gently sloping idealized ocean. Resolution on Georges Bank, for example, is of order 3 km and approaches 2 km across the steep northern flank.

Several studies of the Gulf of Maine and especially Georges Bank have now been completed with this mesh. Lynch and Naimie (1993) studied three-dimensional tidal rectification; Ridderinkhof and Loder (1994) examined Lagrangian trajectories in the tidally rectified flow; Greenberg (1994) examined the dynamic response to wind at various frequencies; and Naimie *et al.* (1994) studied composite seasonal mean circulation fields for six two-month periods using climatological wind and density data. The flow fields from these studies have in turn been used in basic studies of advective influences on early life stages for cod (Werner *et al.*, 1993b; Lough *et al.*, 1994) and scallops (Tremblay *et al.*, 1994). All of these studies use the basic diagnostic FEM approach of Lynch *et al.* (1992) and employ iteration in the frequency domain to achieve a nonlinear solution. The speed and simplicity of this approach have allowed rapid evaluations of basic physical and biological relationships which have proven extremely insightful. The diagnostic simplification of the physics carries, of course, a concomitant penalty in physical realism.

Below we describe results of prognostic time-domain simulations on the same mesh. We first examine some key nonlinear processes on the real Gulf topography. Then we display complete circulation fields obtained under composite climatological forcing. Unless noted otherwise, the simulations use $\tau_0 = 2.0 \times 10^{-4}$, $C_d = 0.005$, $\xi_b = 1.0$ m, $\xi_s = 0.0$, $\Delta z_b = 1.0$ m; vertical meshing according to equation (22); and a single mass variable (density).

5. PROCESS RESULTS

5.1. *Tide*

As a starting point, simulations of the M_2 tide were carried out under constant density and forced as in Lynch and Naimie (1993). As expected, elevation results were essentially unchanged and velocity profiles were more highly sheared near the bottom. Using the same database and error measures, the average elevation deviation was 2.3 cm for amplitude and 4° for phase. For the 48 sites with data records longer than 60 days, the average velocity ellipse deviations were (6.5, 5.5) cm s^{-1} for the major and minor axes, and (10°, 11°) for phase and orientation. No efforts have been made to fine-tune the tidal solution.

5.2. *Barotropic tidal rectification*

In Fig. 3 we show the Eulerian circulation on Georges Bank under M_2 tidal forcing alone, averaged over one tidal cycle and over the water column. As discussed in Lynch and

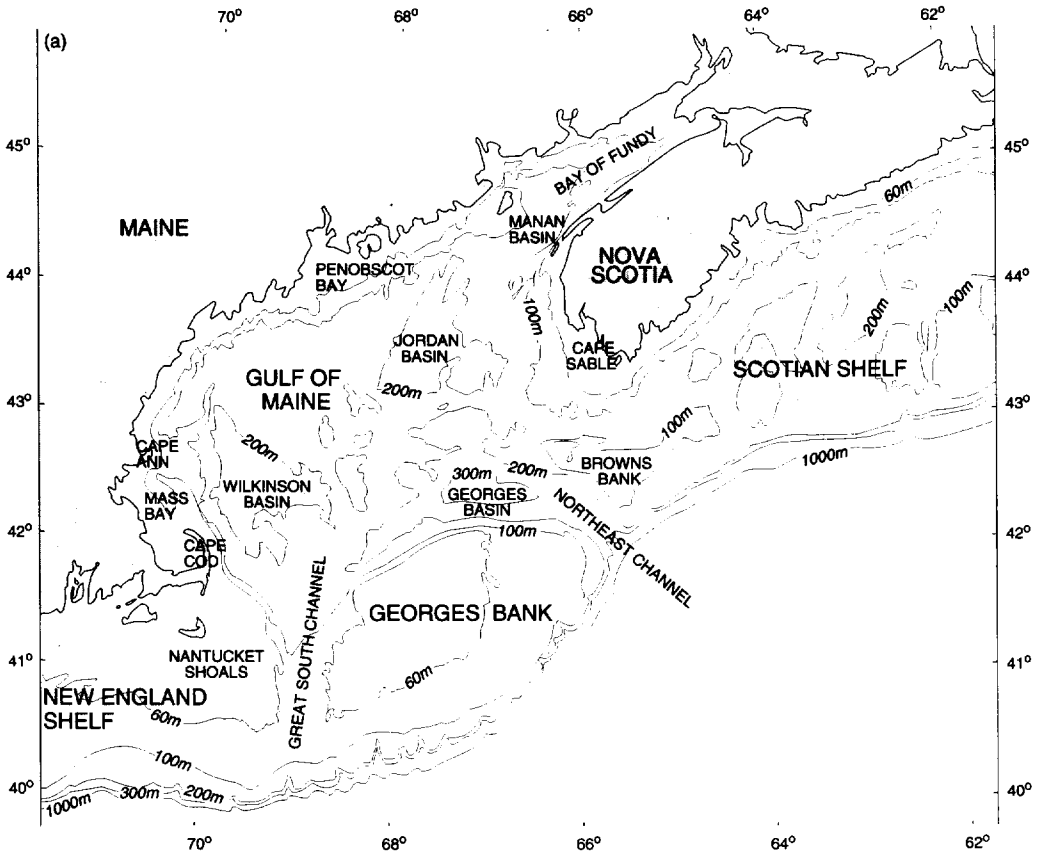

Fig. 1. (a) The topography of the Gulf of Maine; (b) the general pattern of nontidal surface circulation, emphasizing inflow from the Scotian Shelf, general Gulf-scale cyclonic flow, anticyclonic flow around Georges Bank, and branch points in the coastal current at Penobscot Bay, Cape Ann, and Cape Cod. (From "The Regional Maine Research Program (RMRP) for the Gulf of Maine: Initial Oceanographic Framework".)

Naimie (1993) and several previous studies, this is a basic point of departure, being a year-round contributor to the Bank circulation. The agreement with previous model results (Lynch and Naimie, 1993) is remarkably good, establishing the general correspondence between the earlier nonlinear frequency-domain and present time-domain approaches. This is especially interesting since the present results use more advanced closure—which is evidently not critical here in the absence of wind and stratification. Recent studies with this model utilizing enhanced (1 km) horizontal resolution reveal well-resolved secondary circulation cells around shoal structures within the 40 m isobath, with speeds of order 5–10 cm s^{-1}, which may be an important retentive mechanism (Lynch *et al.*, 1995).

5.3. *Stratified tidal rectification*

The above results are quite sensitive to stratification in the frontal region of Georges Bank (Naimie *et al.*, 1994). In Fig. 4 we show the equivalent of Fig. 3, except with surface

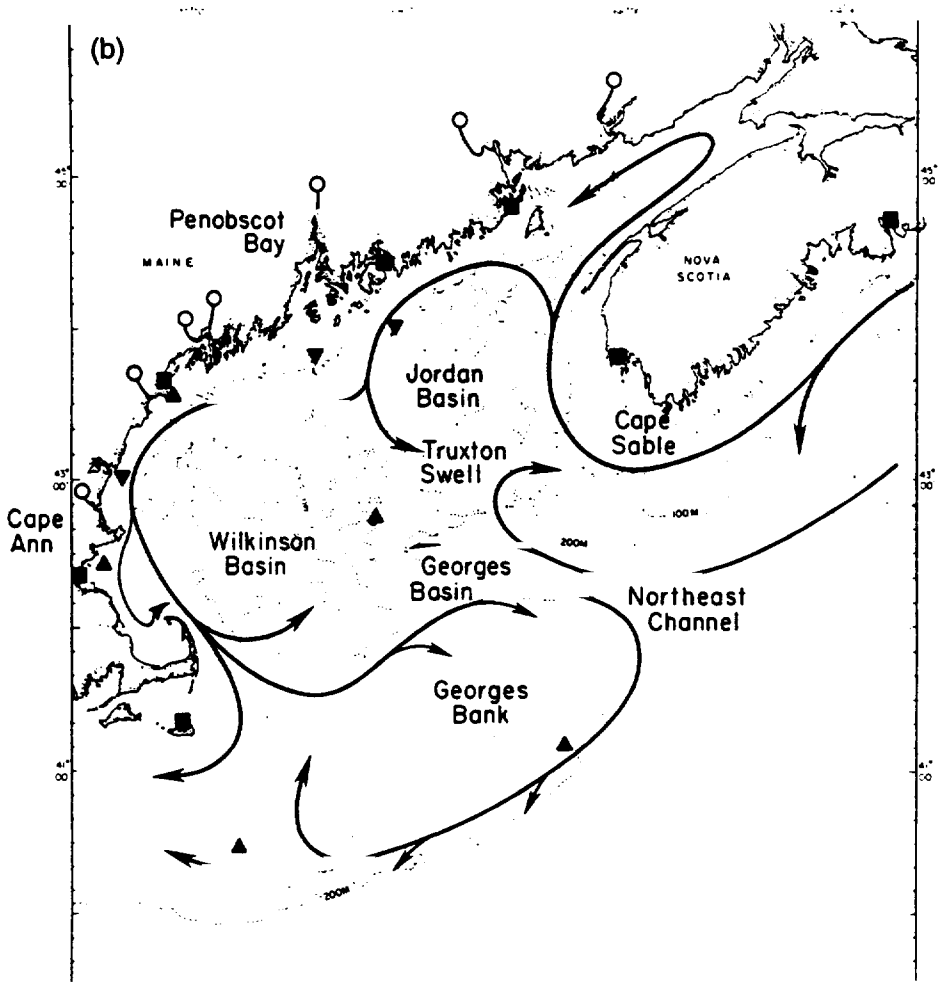

Fig. 1. (*Continued*)

heating sufficient to force a $3\sigma_t$ stratification in the bank area, typical of summer conditions. Apparent is a significant southwestward extension of the recirculation zone in the vicinity of the Great South Channel. Werner *et al.* (1993b) and Tremblay *et al.* (1994) have highlighted the importance of seasonally intensified recirculation in this area to the retention of cod and scallop larvae on the bank. In addition to enhanced retention, there is a significant increase in speed, especially on the northern flank of the Bank. Peak velocities in this location increase from $0.125\ \mathrm{cm\ s^{-1}}$ in the barotropic case to $0.35\ \mathrm{cm\ s^{-1}}$ in the stratified case. Observational evidence of seasonal intensification of this feature is well-established (see e.g. Loder and Wright, 1985; and Loder *et al.*, 1992). Related calculations generally corroborate the finding of Naimie *et al.* (1994) that much of the speed-up is due to the reduction in viscosity accompanying the stratification.

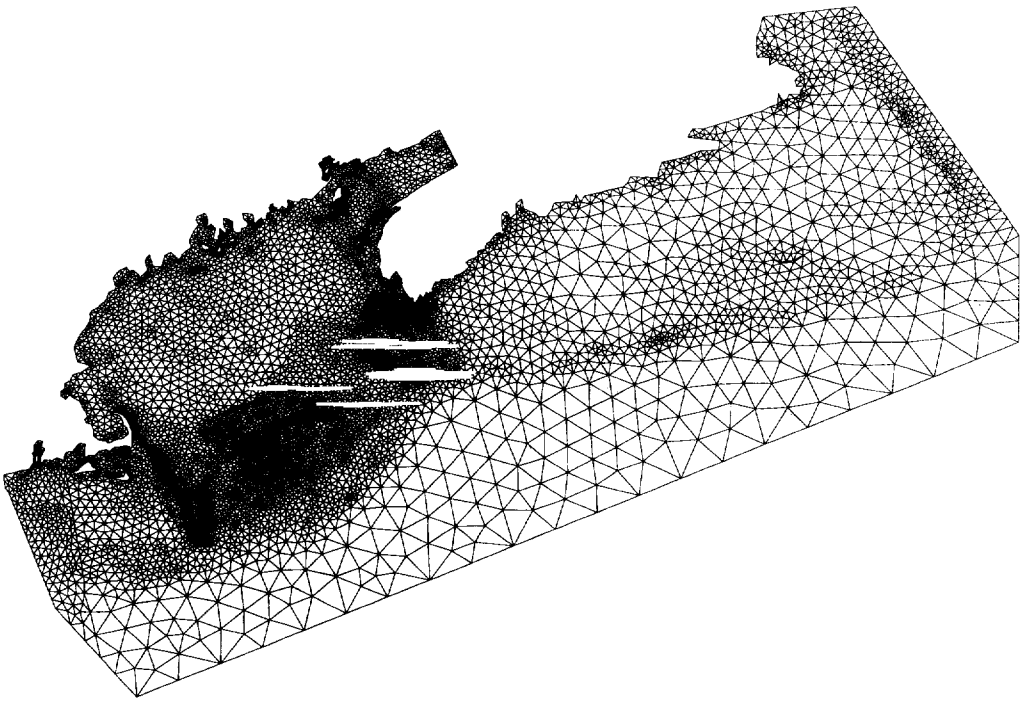

Fig. 2. Horizontal finite element mesh ("G2S") discretizing the Gulf of Maine and Scotian Shelf using linear triangles.

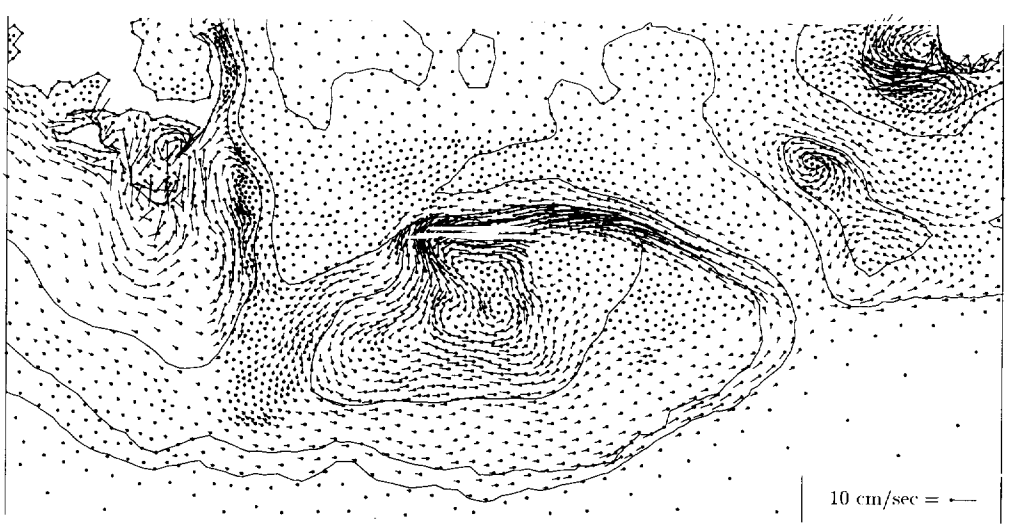

Fig. 3. Vertically averaged tidal residual current at Georges Bank, forced with tide only. Throughout, vectors are displayed with tail marked as a dot.

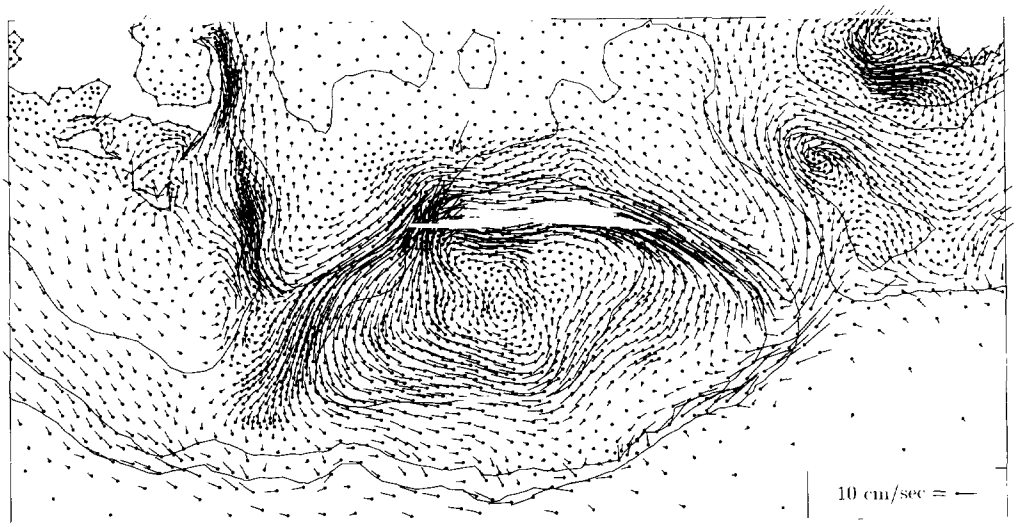

Fig. 4. Same as Fig. 3, but forced with tide and surface heating.

5.4. *Frontal structure*

Figure 5 shows a transect across the northern flank of Georges Bank for the stratified case described above.* The transect cuts across the intense eastward jet visible in Fig. 4 north of the bank. A complex frontal structure is apparent, changing from stratified conditions off-bank to well-mixed conditions on the bank top where tidal velocities are highest and the resulting turbulent mixing is strongest. The location of the mixing front is in good agreement with observation and theory (Loder and Greenberg, 1986; Lynch and Naimie, 1993). A complex cross-bank velocity pattern accompanies the intensified along-bank jet. Figures 6(a) and (b) show the turbulent energy and resulting eddy viscosity profiles on this transect at one point in tidal time. The increasing vertical penetration of the bottom boundary layer with position on-bank is evident, with turbulent energy peaking at the bottom. As expected, eddy viscosity peaks above the bottom, below which it decays to zero in an asymptotically linear manner, due to the mixing length limitation near the bottom. Finally, Fig. 7 shows, again on the same transect, the density structure at two points in tidal time, separated by 6.2 h. Corresponding to the tidal excursion, there is an approximately 10 km cross-bank migration of isopycnals on the bank top. On the sides of the bank this generates vertical isopycnal motions of order 20 m, which propagate away from the bank.

5.5. *Wind-driven mixed layer*

In a separate set of experiments, we apply a uniform wind instantaneously to the model after it has achieved dynamic equilibrium with the tide (wind stress is 0.1 Pascal, directed towards 118.5° clockwise from true north). The near-surface response over two of the deep basins of the Gulf appears in Fig. 8, for the barotropic case. It is apparent that the

*This is the same "NF" transect used by Naimie *et al.* (1994).

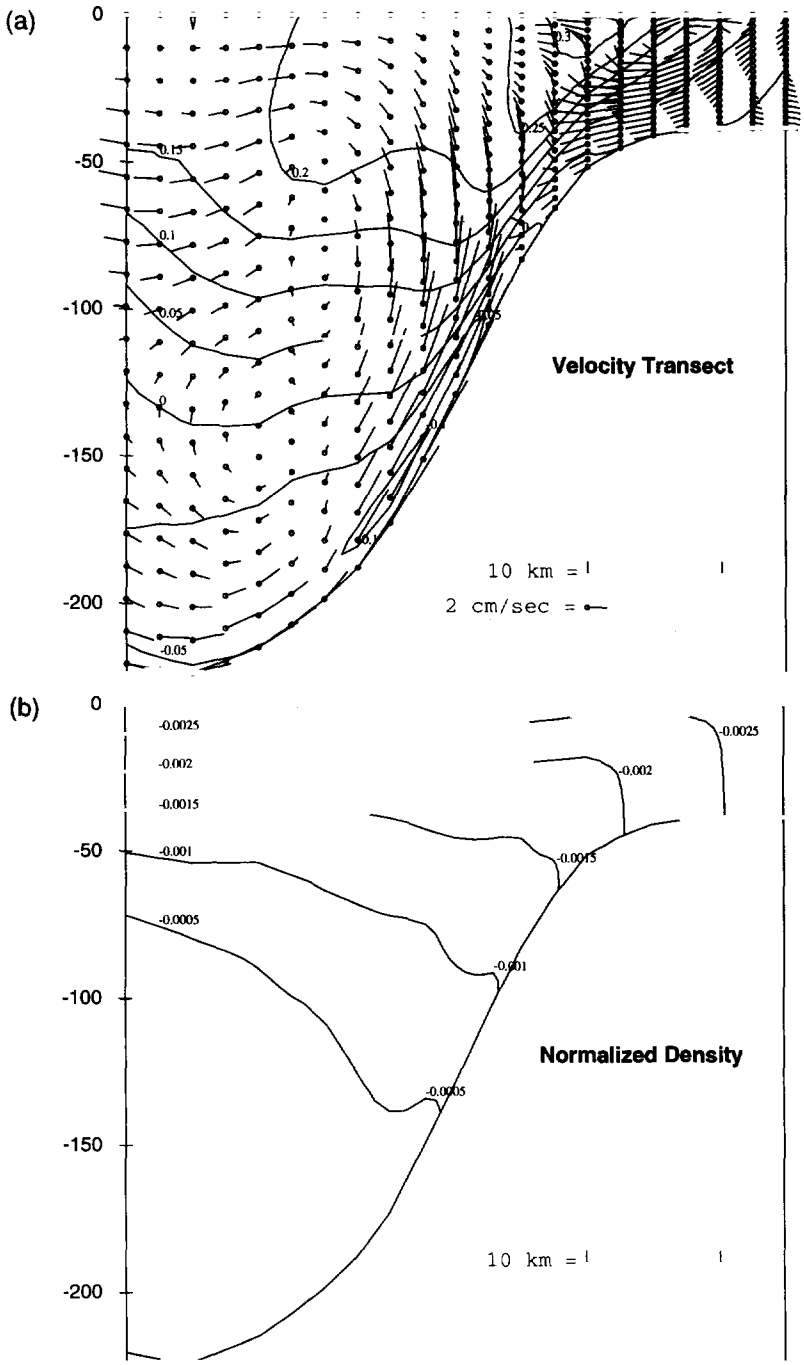

Fig. 5. Tidally averaged vertical transect across the northern flank from the stratified case of Fig. 4, showing the density profile changing from stratified off-bank to well-mixed on the bank top. (a) Along-bank current speed (isotachs) and cross-bank velocity (tail-marked vectors); (b) contours of density anomaly, $(\rho - \rho_0)/\rho_0$. Depth scale is meters.

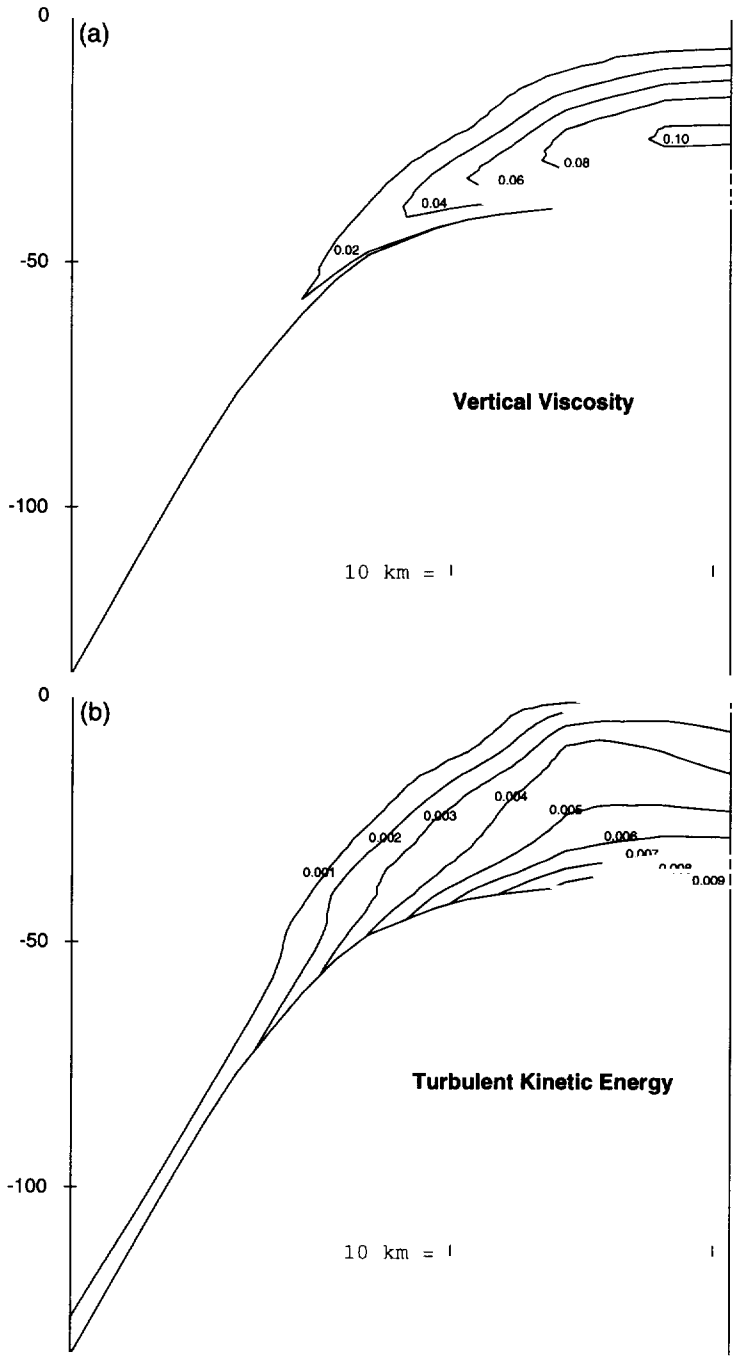

Fig. 6. Tidal time transect across the northern flank from the stratified simulation (Fig. 4) showing the increasing vertical penetration of the bottom boundary layer with position on-bank. (a) Contours of vertical eddy viscosity, increasing from the surface to a maximum, and dropping off near-bottom where mixing length is limited (top figure); (b) contours of q^2, increasing monotonically from the surface to bottom (bottom figure); MKS units are indicated.

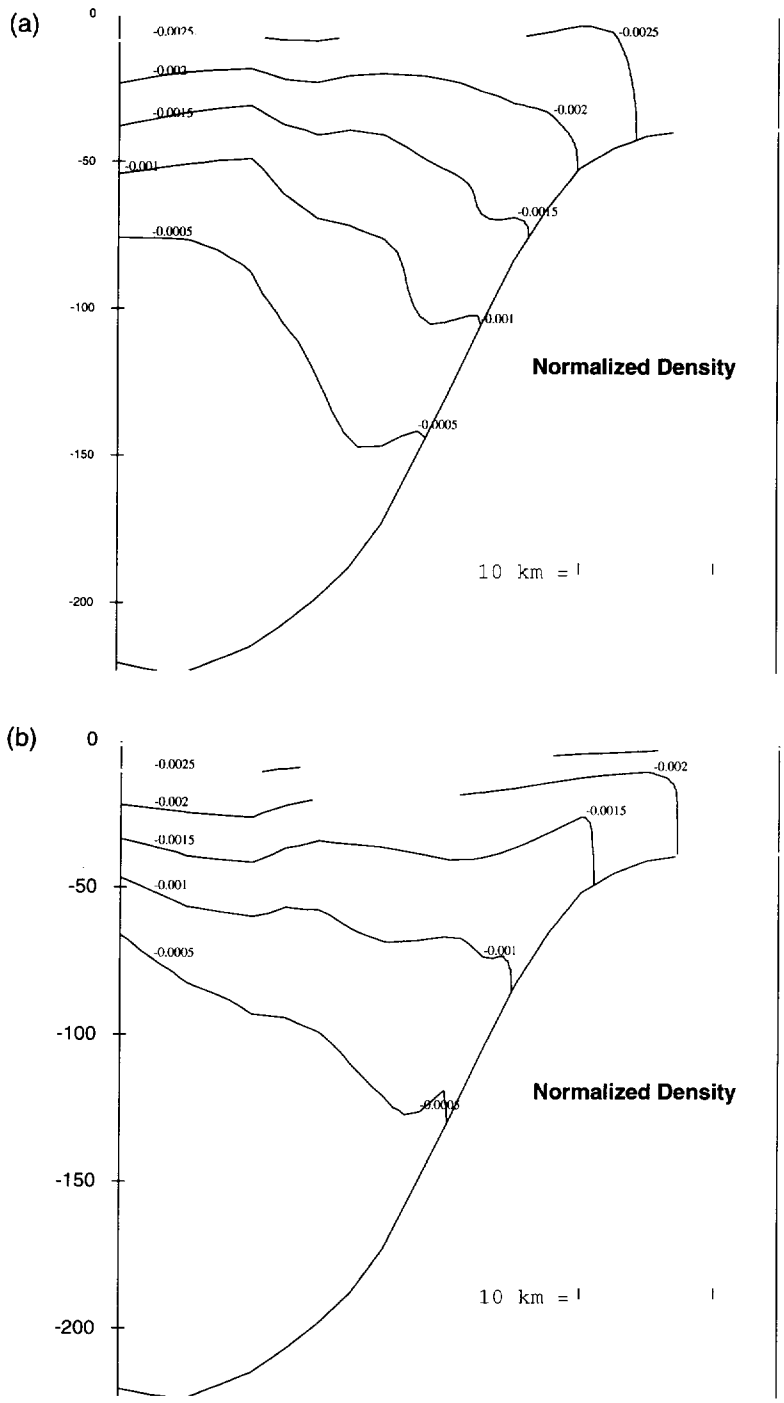

Fig. 7. Tidal time vertical transects across the northern flank from the stratified simulation showing advection of density structures. The two figures are separated by 6.2 h. Density is reported as $(\rho - \rho_0)/\rho_0$; depth scale is in meters.

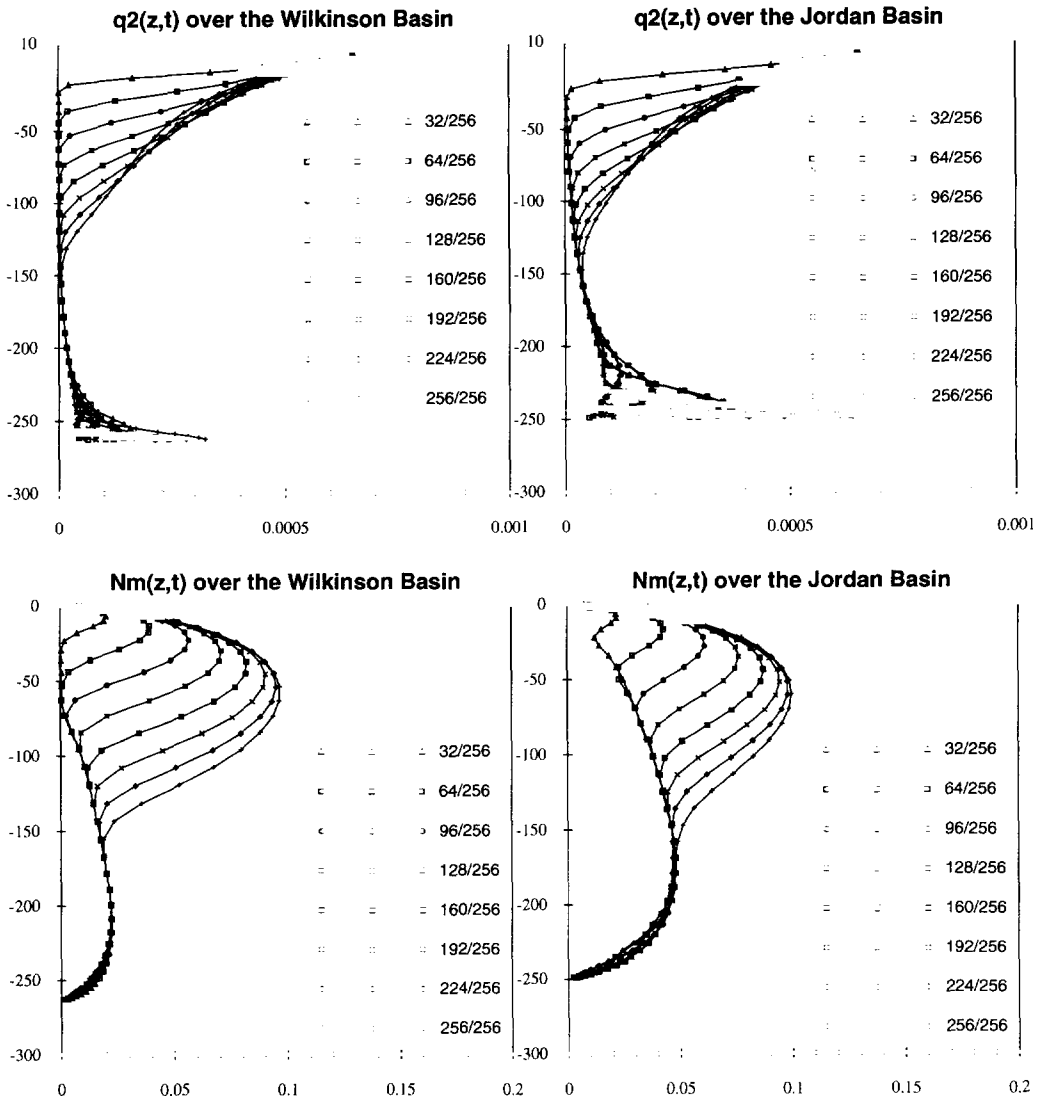

Fig. 8. Wind-deepening calculation: constant density case. Turbulent kinetic energy q^2 and vertical viscosity N_m are shown vs z over the Wilkinson and Jordan Basins. Time indicated is the fraction of one M_2 period from onset of the wind; $l = 0.4$ at the surface; MKS units.

responses are identical except for the bottom boundary layer, which is due to the difference in the barotropic tide at the two locations. Apparent in these unstratified results is the very deep penetration of the wind influence. In Fig. 9, the influence of initially uniform, linear stratification ($\Delta\rho = 0.5\sigma_t$ over 100 m) is shown. The reduction in penetration is dramatic, and in agreement with experiment (the Price (1979) relation gives $h = 18.7$ at $t = 6.2$ h).*

*These results were obtained with $\xi_s = 1$ m. Use of $\xi_s = 0$ gives anomalous early-time results in these cases.

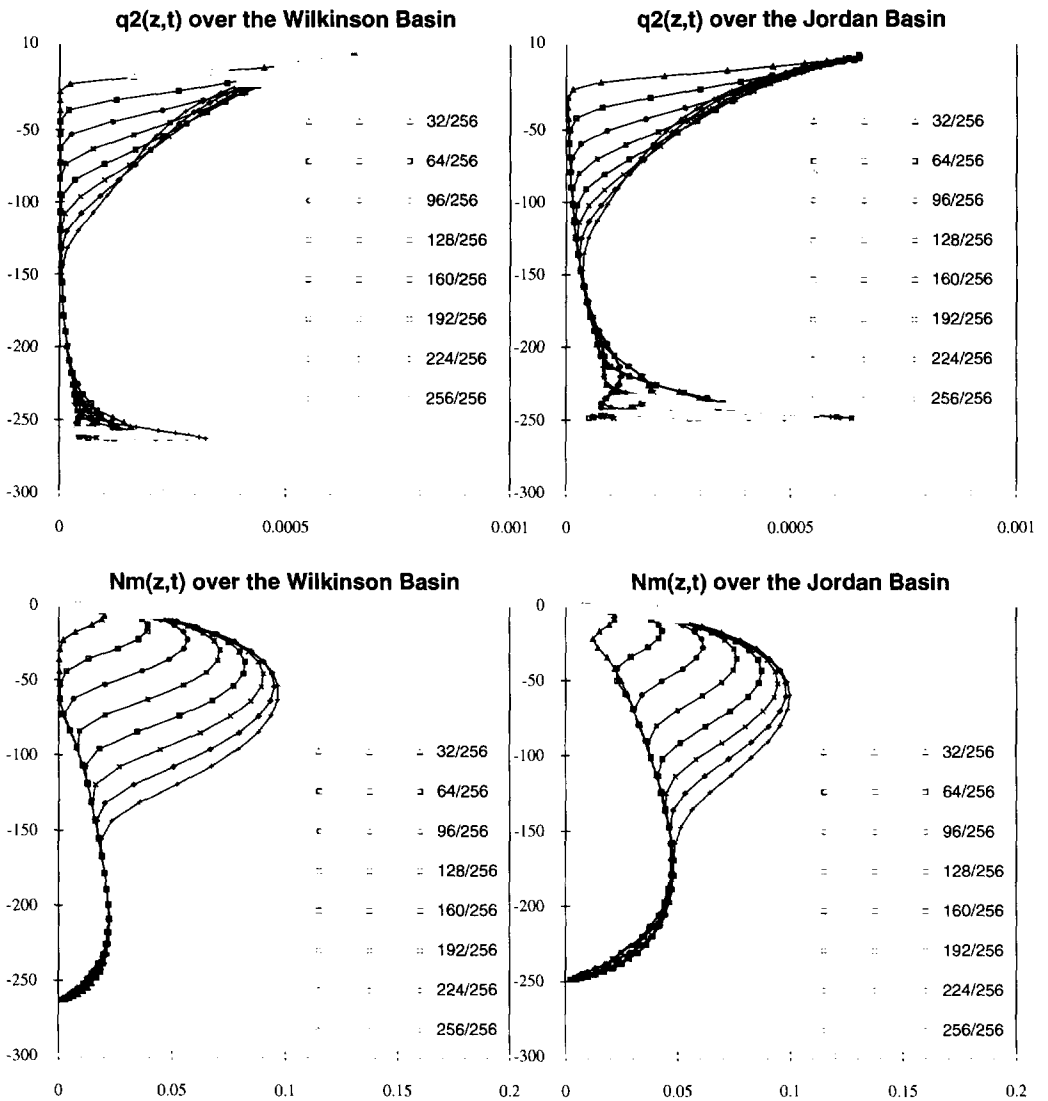

Fig. 8. Wind-deepening calculation: constant density case. Turbulent kinetic energy q^2 and vertical viscosity N_m are shown vs z over the Wilkinson and Jordan Basins. Time indicated is the fraction of one M_2 period from onset of the wind; $l = 0.4$ at the surface; MKS units.

responses are identical except for the bottom boundary layer, which is due to the difference in the barotropic tide at the two locations. Apparent in these unstratified results is the very deep penetration of the wind influence. In Fig. 9, the influence of initially uniform, linear stratification ($\Delta\rho = 0.5\sigma_t$ over 100 m) is shown. The reduction in penetration is dramatic, and in agreement with experiment (the Price (1979) relation gives $h = 18.7$ at $t = 6.2$ h).*

*These results were obtained with $\xi_s = 1$ m. Use of $\xi_s = 0$ gives anomalous early-time results in these cases.

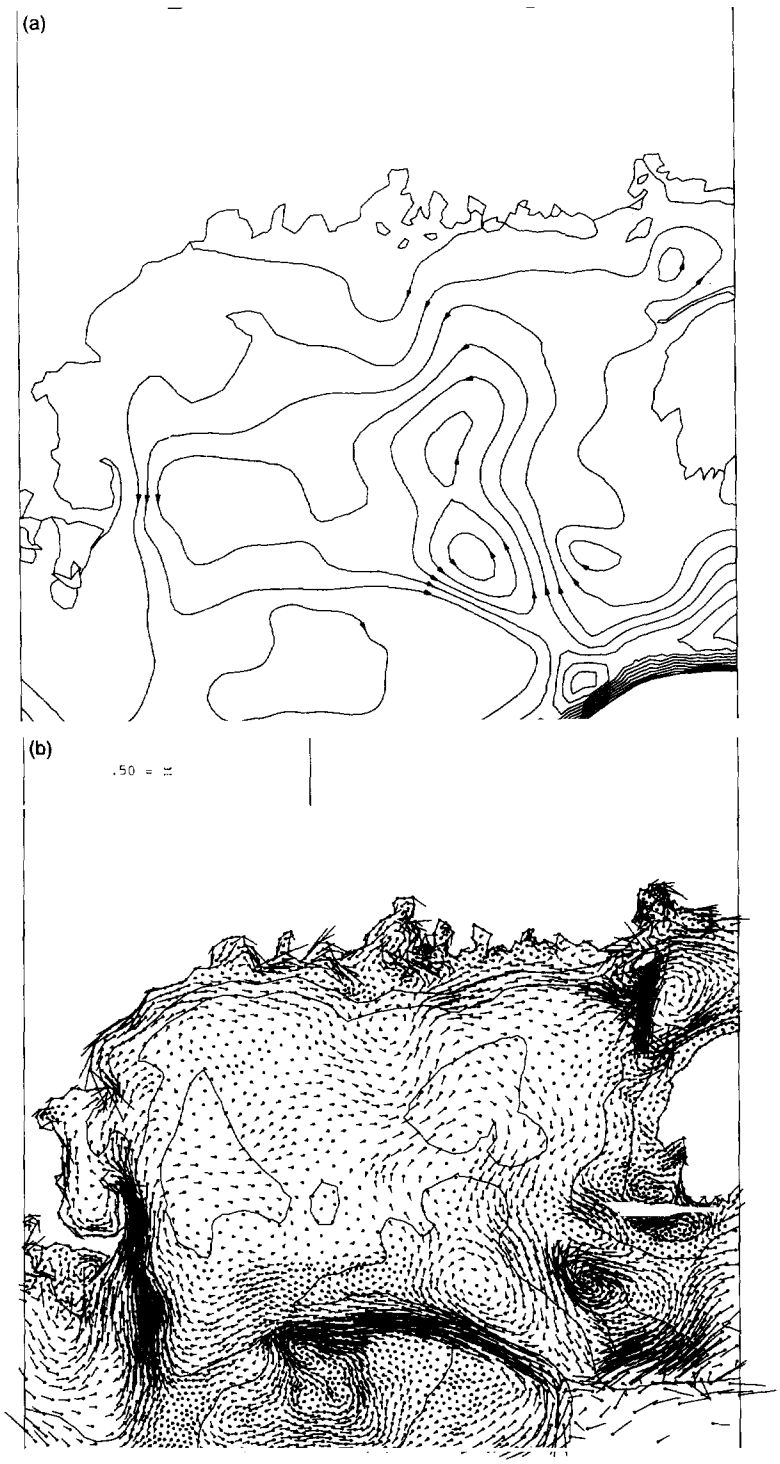

Fig. 10. The Gulf-wide, tidally averaged circulation in March–April. (a) Stream function, contour spacing 0.1 Sv (top figure); (b) vertically averaged velocity (bottom figure).

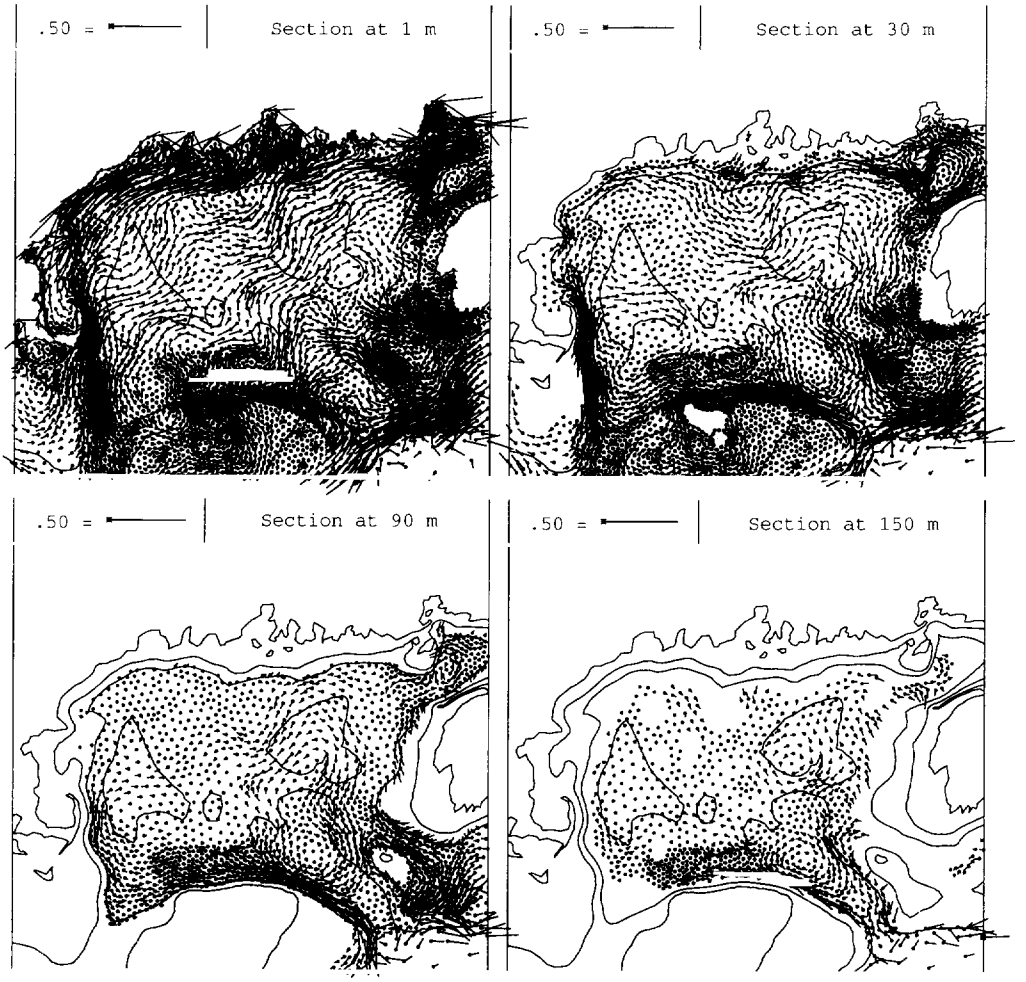

Fig. 11. March–April velocity patterns on level surfaces at 1, 30, 90 and 150 m below the surface.

base (Woodruff *et al.*, 1987), averaged over the period 1946–1979, from shipboard measurements. Stresses were computed using the approximation method of Wright and Thompson (1983) and the neutral-stability, speed-dependent drag coefficients of Isemer and Hasse (1987). These show strong seasonal modulation. For example in March–April, the average stress is 0.0472 Pa, toward 121.4° clockwise from true north; while the July–August average is 0.0138 Pa, toward 51.0° (Naimie *et al.*, 1994).

Mass field. Climatological (T, S) fields were obtained for the same two-month periods from the Canadian AFAP database, which spans the period 1912–1991, with greatest coverage from 1961 forward. This archive provides 10,000–20,000 bottle or CTD profiles per two-month averaging period within the model domain. The specific estimates of climatological mean density are obtained by four-dimensional space–time optimal interpolation following Bretherton *et al.* (1976) with locally variable

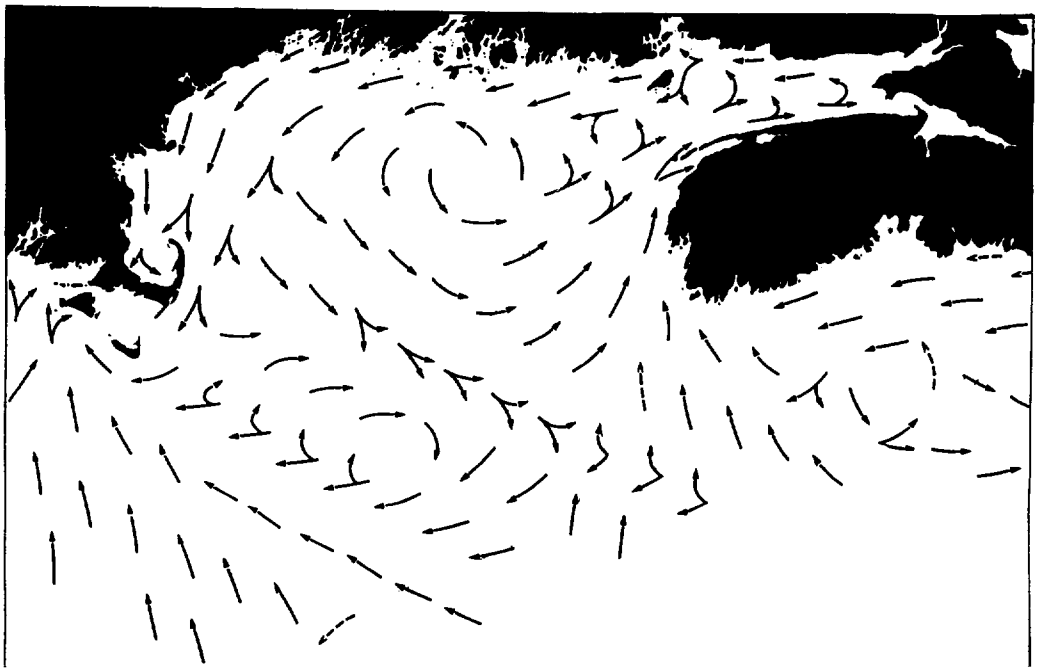

Fig. 12. Composite of observed surface drift, for Spring, from Bumpus and Lauzier (1965).

correlation scales, of order 30–40 km (horizontal), 15–30 m (vertical) and 30–45 days (temporal). These fields and associated diagnostic circulation fields are examined in detail in Hannah and Loder (1994) and Loder *et al.* (1995).

The prognostic model was initialized with the climatological mass field, and in addition with seasonal pressure and current derived diagnostically in Naimie *et al.* (1994). The model was then driven by the M_2 tide and residual elevation at the open boundary and by the seasonal mean wind stress. At the free surface, the density was nudged toward its climatological mean as in equation (14) with $\alpha = 2.3 \times 10^{-5}$ m s^{-1}. Following spin-up, the tidal time results were averaged over a tidal cycle. The streamfunction ψ was computed as in Lynch and Naimie (1993):

$$\nabla^2\psi = -\nabla \times \left[\frac{1}{T}\int_t^{t+T}\int_{-h}^{\zeta} \mathbf{v}\, dz\, \mathrm{d}t\right] \tag{23}$$

with T the tidal period.

Herein we present the computed circulation features from a Gulf-wide perspective. Naimie (1995) provides an in-depth examination of Georges Bank and the importance of advanced turbulence closure and density evolution on the circulation for these bimonthly periods.

6.1. *March–April*

In Figs 10 and 11 we show the computed circulation pattern in March–April. There are several important features of this simulation.

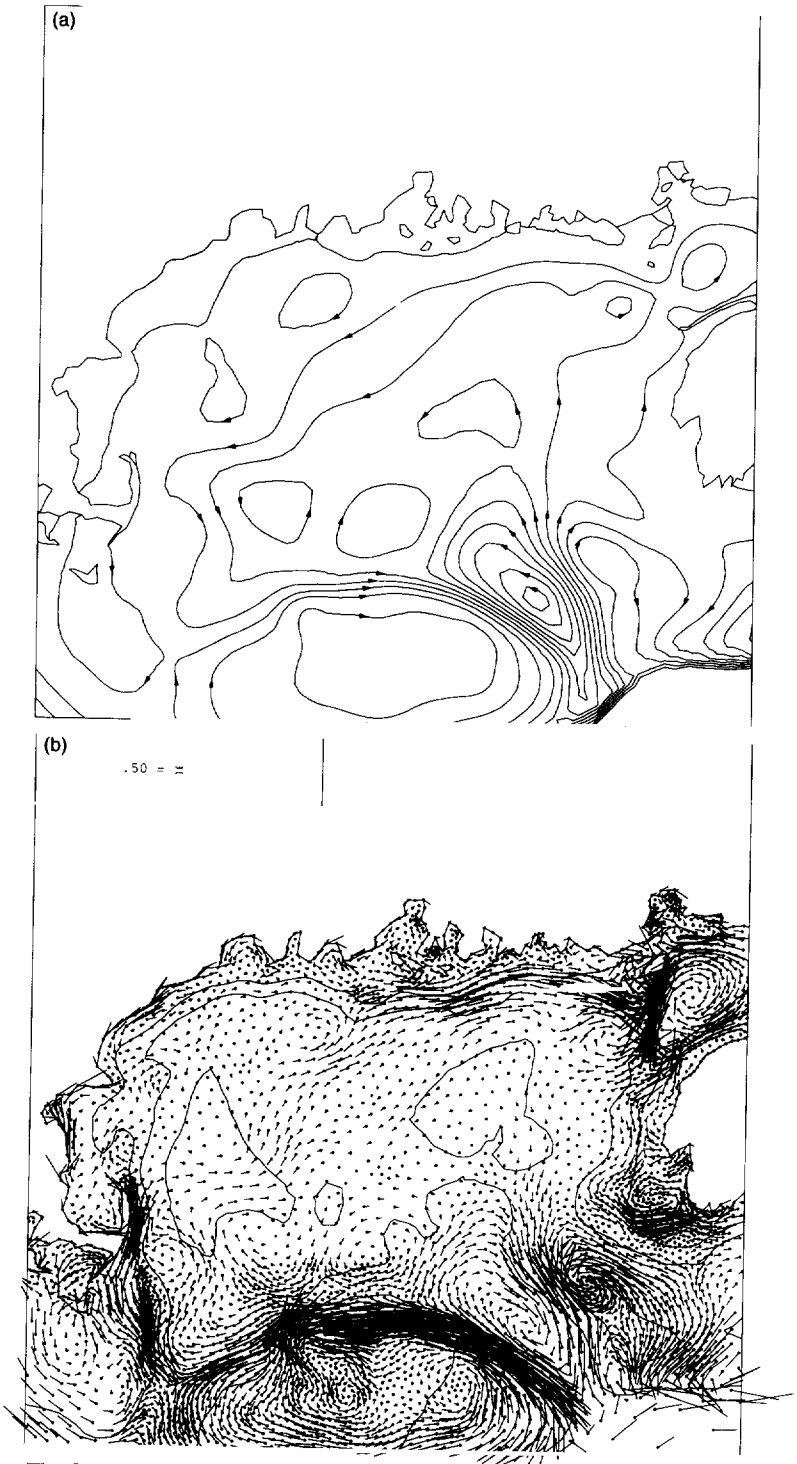

Fig. 13. The Gulf-wide, tidally averaged circulation in July–August. (a) Stream function, contour spacing 0.1 Sv (top figure); (b) vertically averaged velocity (bottom figure).

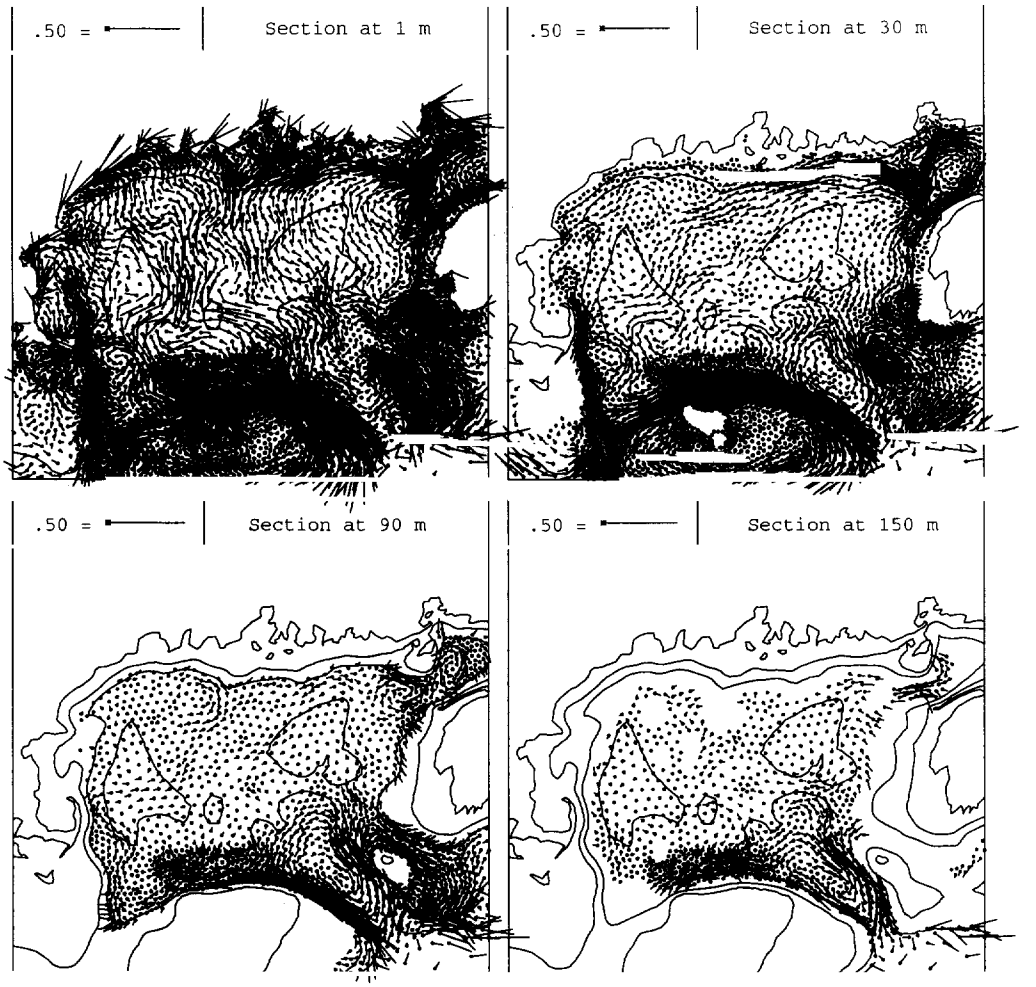

Fig. 14. July–August velocity patterns on level surfaces at 1, 30, 90 and 150 m below the surface.

A dominant circulation feature is in the eastern Gulf, where a pronounced cyclonic gyre occurs over Jordan and Georges Basins. The recirculating transport in this gyre is approximately 0.3 Sv (0.3×10^6 m^3 s^{-1}). Such a central Gulf feature has been identified in essentially every circulation study of the Gulf since Bigelow (1927). (See Pettigrew, 1994 for a recent review.) Its dynamical origin lies in the large-scale baroclinicity. The velocity plots reveal two separate deep gyres over the two basins, which are merged. Unrelated to these is a separate gyre over Grand Manan Basin, which results from barotropic tidal rectification.

Along the shoreward boundary is a well-developed coastal current. In the eastern Gulf, this current is the northern extent of the Jordan Basin gyre described above. It departs from the coast south of Penobscot Bay with only a portion returning to the coast. This is the first important coastal branch point. Further west, a second branch point is found at Cape

Ann, where a portion of the coastal current enters and circuits Massachusetts and Cape Cod Bays. Further downstream, there is third branch point east of Cape Cod, where a portion of the flow (0.1–0.2 Sv) is diverted east to the northern flank of Georges Bank, with the balance exiting the Gulf through the Great South Channel.

East of Cape Cod, a cyclonic gyre occurs in the topographic cul-de-sac north of Great South Channel. This feature is most pronounced at intermediate depth (e.g. the 30 m section in Fig. 11). The coastal current–Georges Bank branch point described above involves the periphery of this gyre.

To the south of the central Gulf, the familiar partly closed gyre surrounding Georges Bank dominates the picture. Such a gyre figures prominently in all studies of the bank (e.g. Naimie *et al.*, 1994). In this lightly stratified season, its principal dynamical origin is in barotropic tidal rectification, consistent with the process studies above. The central Gulf gyre merges with this feature along the northern flank and enhances the along-bank transport there. Other familiar features appear along the bounding banks—for example, the upwelling off south-west Nova Scotia, which is present in essentially all model runs and thought to be the year-round result of topographic tidal rectification (Tee *et al.*, 1993).

Overall, these features are qualitatively consistent with Fig. 1(b)—admittedly a vague standard of comparison based on consensus opinion. In Fig. 12 we reproduce the surface circulation pattern from Bumpus and Lauzier (1965), which summarizes surface drift observations during March–April–May over many years. Our results are in broad general agreement. The considerable baroclinic structure in the computed result reveals complexity in the deep transport pathways which remain still largely speculative.

6.2. *July–August*

In Figs 13 and 14 we show the computed circulation for July–August. The general features of March–April are still present—a dominant cyclonic gyre in the central gulf, a complex coastal current system, and an anticyclonic recirculation around Georges Bank. The details are changed, however, reflecting the onset of summer stratification and the evolution and migration of the water masses in the deep basins.

The eastern Gulf gyre identified in March–April has both intensified and spread eastward. The Georges Basin portion is now clearly a separate feature, with recirculation strengthened to roughly 0.5 Sv. This now forms the core of a larger cyclonic structure which spreads into the western Gulf, beyond the confines of Jordan Basin. Outside of this enlarged gyre, the western Gulf exhibits considerable complexity.

The coastal current has also undergone seasonal change. In accord with the westward spreading of the Jordan Basin gyre, the Penobscot branch point has shifted westward, with the flow diverted toward Wilkinson Basin and a negligible portion returning to the coast. At Cape Ann, there is a significant reduction in the transport into Massachusetts Bay, accompanied by a reversal or nullification of the local March–April gyre in the Bay.

The Georges Bank circulation has intensified, in accord with enhanced seasonal stratification as in Naimie *et al.* (1994) and consistent with the process studies described above. Notable is the intensification of the northern flank flow, and the strengthening and westward migration of the northward recirculation zone at Great South Channel. Details of the Georges Bank circulation and frontal structure are reported in Naimie (1995).

Like the previous season, these results are broadly consistent with the prevailing

knowledge of the Gulf-wide circulation. The differences between the two patterns are complex and significant and suggest numerous avenues of scientific inquiry.

7. SUMMARY

We have demonstrated the synthesis of a comprehensive coastal/shelf circulation model. The FEM provides the essential spatial ingredients: broad geographic coverage with flexible local resolution both horizontally and vertically. The incorporation of turbulence closure and fully prognostic mass field evolution in tidal time brings the internal physical processes to state-of-the-art for hydrostatic shelf modeling. The examples demonstrate a broad range of circulation features representing important nonlinear interactions among shelf physics and detailed topography.

These results have been achieved with conventional, simple finite element technology—our goal has been to establish a baseline of FEM capability and performance, against which future advances may be evaluated. There is no doubt that the inclusion of more advanced FEM concepts will bring enhanced realism—for example, the use of Lagrangian and/or spectral methods for the handling of advection. We expect the present model will serve as an experimental platform for such enhancements. Additionally, we look forward to advances in the general areas of open boundary conditions; data assimilation and operational use with limited data support; representation of boundary layer interactions at the benthic and air–sea interfaces; and continued general progress in turbulence closure. Of particular interest are the generic modeling issues surrounding computation of the baroclinic pressure gradient on terrain-following coordinate systems.

The exploratory Gulf of Maine results show considerable promise as a framework for scientific research. In particular, the seasonal mean results represent the first truly comprehensive model solution for the Gulf; and all major circulation features are present. It would be senseless however to assert "agreement" with observation here, given the complexity of the phenomena and the sparsity of the observational data base. Instead, we assert the validity of the mathematical product, and advance it as a candidate for plausible climatology. There remain dozens of specific aspects of the circulation which deserve detailed scrutiny, and hopefully the present solutions will be but the first of a series with increasing quality, with accompanying advances in knowledge of the Gulf circulation.

We see five important areas for future model-assisted research:

(1) the *coastal current* including the dynamic interaction of local (i.e. local wind and river discharge) and large-scale (i.e. Jordan Basin gyre) physical features, and their influence on the location and strength of the various branch points;
(2) *Georges Bank*, where the details of the frontal structure and its seasonal modulation are critical to several important biological processes;
(3) *Scotian Shelf/Northeast Channel exchanges*—including the relative roles of wind, baroclinicity, along-shelf transport, and Gulf Stream features in regulating these critical exchanges;
(4) *deep basins*—circulation, exchange, and water mass evolution, and the role of these processes in controlling the large-scale circulation in the Gulf;
(5) *shelf/slope coupling* and the incorporation of realistic variability originating seaward of the shelf-break front.

We look forward to continued development of the FEM in this context; its use and

scrutiny by colleagues in a variety of scientific investigations; and the ultimate transfer of useful models to operational agencies. It is hoped that the twin goals of basic algorithmic advances, coupled with site-specific studies, will result in the availability and effective use of comprehensive circulation models for the Gulf and other shelf regions on a timely basis.

Acknowledgements—We thank our colleagues: David Greenberg, for providing tidal and bathymetric data and generous access to previous Gulf of Maine modeling experiences; John Loder, for providing the climatological data base and invaluable physical advice over an extended period of time; Peter Smith, David Brooks and Wendell Brown, for many helpful discussions; and Monica Holboke, Matthias Johnsen and Elizabeth Wolff for assistance in constructing the computational results. Financial support from the National Science Foundation, the Office of Naval Research, the Joint NSF–NOAA GLOBEC program, the Gulf of Maine Regional Marine Research Program and the New Hampshire Sea Grant College Program is gratefully acknowledged. This is Contribution No. 21 of the U.S. GLOBEC Program.

REFERENCES

Bernier C. (1990) Etude et parallelisation d'un code elements finis pour la modelisation quasi-geostrophique des circulations oceaniques. Ph.D. Dissertation, Thèse de l'institut National Polytechnique de Grenoble, Grenoble, France.

Bigelow H. B. (1927) Physical oceanography of the Gulf of Maine. *Bulletin—U.S. Bureau of Fisheries*, **40**, 511–1027.

Blain C. A., J. J. Westerink and R. A. Luettich Jr (1994) The influence of domain size on the response characteristics of a hurricane storm surge model. *Journal of Geophysical Research*, **99** (C9), 18467–79.

Blumberg A. and G. L. Mellor (1987) A description of a three-dimensional coastal ocean circulation model. *Three-Dimensional Coastal Models*, N. S. Heaps, editor, American Geophysical Union, Washington D.C. Coastal and Estuarine Series **4**, 1–16.

Blumberg A. F., B. Galperin and D. J. O'Connor (1992) Modeling vertical structure of open-channel flows. *ASCE Journal of Hydraulic Engineering*, **118**, 1119–1134.

Bretherton F. P., R. E. Davis and C. B. Fandry (1976) A technique for objective analysis and design of oceanographic experiments applied to MODE-73. *Deep Sea Research*, **23**, 559–582.

Bumpus D. F. and L. M. Lauzier (1965) Surface circulation on the continental shelf of eastern North America between Newfoundland and Florida. *American Geographical Society*, Serial Atlas of the Marine Environment, Folio 7.

Canceill P., R. Agelou and P. Vincent (1994) Barotropic tides in the Mediterranean Sea from a finite element numerical model. *Journal of Geophysical Research* (in press).

Fix G. J. (1975) Finite element models for ocean circulation problems. *SIAM Journal of Applied Mathematics*, **29**, 371–387.

Foreman M. G. G. (1983) An analysis of the "Wave Equation" model for finite element tidal computations. *Journal of Comput. Physics*, **52**, 290–312.

Foreman M. G. G. (1991) Barotropic tides and tidal residuals for the southwest coast of Vancouver Island. *Tidal hydrodynamics*, B. B. Parker, editor, Wiley, NY, pp. 109–124.

Foreman M. G. G., A. M. Baptista and R. A. Walters (1992a) Tidal model studies of particle trajectories around a shallow coastal bank. *Atmosphere–Ocean*, **30**, 43–69.

Foreman M. G. G., R. F. Henry, R. A. Walters and V. A. Ballantyne (1993) A finite element model for tides and resonance along the north coast of British Columbia. *Journal of Geophysical Research*, **98** (C2), 2509–2531.

Foreman M. G. G., R. E. Thomson, D. R. Lynch and R. A. Walters (1992b) A finite element model for three-dimensional flows along the west coast of Vancouver Island. *Estuarine and Coastal Modeling, Proceedings of the 2nd International Conference*, M. L. Spaulding *et al.*, editors, ASCE, NY, pp. 574–585.

Foreman M. G. G. and R. A. Walters (1990) A finite-element tidal model for the southwest coast of Vancouver Island. *Atmosphere–Ocean*, **28**, 261–287.

Galperin B., L. H. Kantha, S. Hassid and A. Rosati (1988) A quasi-equilibrium turbulent energy model for geophysical flows. *Journal of Atmospheric Science*, **45**, 55–62.

Genco M.-L. (1993) Les marees dans l'Ocean Atlantique: modelisation et bilan energetique, Ph.D., l'Université Joseph Fourier, Grenoble I, France.

Gill A. E. (1982) *Atmosphere–Ocean Dynamics*, Academic Press, pp. 599–603.

Gray W. G., J. Drolet and I. P. E. Kinnmark (1987) A simulation of tidal flow in the southern part of the North Sea and the English Channel. *Advances in Water Resources*, **10**, 131–137.

Greenberg D. A. (1994) Model Progression in the Gulf of Maine. In: Proceedings of the RARGOM Circulation Modeling Workshop, Dartmouth College, Hanover, New Hampshire, Oct. 1993, RARGOM Report No. 94-1.

Greenberg D. A. and D. R. Lynch (1992) Review: Gulf of Maine circulation modeling. In: Proceedings of the Gulf of Maine Scientific Workshop, Woods Hole, Massachusetts, J. Wiggin and C. N. K. Mooers, editors, Urban Harbors Institute, U. Mass., Boston, pp. 125–140.

Grotkop G. (1973) Finite element analysis of long-period water waves. *Computer Methods in Applied Mechanics and Engineering*, **2**, 147 ff.

Haidvogel D. B., A. R. Robinson and E. E. Schulman (1980) The accuracy, efficiency, and stability of three numerical models with application to open ocean problems. *Journal of Comput. Physics*, **34**, 1–53.

Hannah C. G. and J. W. Loder (1994) Seasonal variation of the baroclinic circulation in the Scotia–Maine region. In: Proceedings of the Seventh International Biennial Conference on the Physics of Estuaries and Coastal Seas, Woods Hole, Mass., Nov. 1994 (submitted 1994).

Henry R. F. (1988) Interactive design of irregular triangular grids. In: *Computational methods in water resources, Vol. II*. Proceedings of the VIIth International Conference, MIT, Boston, U.S.A., June 1988, M. A. Celia *et al.*, editors, Computational Mechanics Publications, Elsevier, pp. 445–450.

Henry R. F. and R. A. Walters (1993) Geometrically-based, automatic generator for irregular triangular networks. *Communications in Applied Numerical Methods*, **9**, 555–566.

Isemer H. J. and L. Hasse (1987) *The Bunker climate atlas of the North Atlantic Ocean, Vol. 2, air–sea interactions*, 252 pp., Springer-Verlag, NY.

Iskandarani M., D. B. Haidvogel and J. P. Boyd (1995) A staggered spectral finite element model with application to the oceanic shallow water equations. *International Journal for Numerical Methods in Fluids*, **20**, 393–414.

Jamart B. M. (1980) Finite element computation of barotropic tidal motion in deep estuaries. Ph.D. Dissertation, University of Washington, Seattle, WA.

Jamart B. M. and J. Ozer (1989) Some results and comments on the tidal flow forum exercise. *Advances in Water Resources*, **12**, 211–221.

Johnsen M. T. and D. R. Lynch (1994) A second-order radiation boundary condition for the shallow water wave equations on two-dimensional unstructured finite element grids. *International Journal for Numerical Methods in Fluids*, **18**, 575–604.

Johnsen M. T. and D. R. Lynch (1995) Assessment of a second-order radiation boundary condition for tidal and wind-driven flows. In: *Quantitative skill assessment for coastal ocean models*, D. R. Lynch and A. M. Davies, editors, Coastal and Estuarine Series **47**, American Geophysical Union, Washington, DC.

Kinnmark I. P. E. (1986) The shallow water wave equations: formulation, analysis and application. *Lecture Notes in Engineering*, **15**, Brebbia and Orszag, editors, Springer-Verlag, Berlin, 187 pp.

Kinnmark I. P. E. and W. G. Gray (1984) A two-dimensional analysis of the wave equation model for finite element tidal computations. *International Journal of Numerical Methods in Engineering*, **20**, 369–383.

Kolar R. L., W. G. Gray, J. J. Westerink and R. A. Luettich Jr (1994a) Shallow water modeling in spherical coordinates: equation formulation, numerical implementation and application. *Journal of Hydraulic Research*, **32**, 3–24.

Kolar R. L., J. J. Westerink, M. E. Cantekin and C. A. Blain (1994b) Aspects of nonlinear simulations using shallow-water models based on the wave continuity equation. *Computers in Fluids*, **23**, 3, 523–538.

Le Provost C. (1986) On the use of finite element methods for ocean modeling. *Advances in Phys. Oceanogr. Numer. Modeling*, J. J. O'Brien, editor, Reidel, pp. 557–580.

Le Provost C., C. Bernier and E. Blayo (1994) A comparison of two numerical methods for integrating a quasi-geostrophic multilayer model of ocean circulations: finite element and finite difference methods. *Journal of Comput. Physics*, **110**, 341–359.

Le Provost C., M.-L. Genco and F. Lyard (1995) Modeling and predicting tides over the world ocean. In: *Quantitative skill assessment for coastal ocean models*, D. R. Lynch and A. M. Davies, editors, Coastal and Estuarine Series **47**, American Geophysical Union, Washington, DC.

Le Provost C. and A. Poncet (1978) Finite element method for spectral modelling of tides. *International Journal of Numerical Methods in Engineering*, **12**, 853–871.

Le Provost C. and P. Vincent (1986) Some tests of precision for a finite element model of ocean tides. *Journal of Computational Physics*, **65**, 273–291.

Le Provost C., P. Vincent, P. Canceill, M. L. Genco and F. Lyard (1991) A new multiple basin model of the world ocean tides. IUGG XXth General Assembly, Vienna.

Loder J. W., D. Brickman and E. P. W. Horne (1992) Detailed structure of currents and hydrography on the northern side of Georges Bank. *Journal of Geophysical Research*, **97** (C9), 14331–14351.

Loder J. W. and D. A. Greenberg (1986) Predicted positions of tidal fronts in the Gulf of Maine region. *Continental Shelf Research*, **6**, 397–414.

Loder J. W., G. Han, C. G. Hannah, D. A. Greenberg and P. C. Smith (1995) Hydrography and baroclinic circulation in the Scotian Shelf region: winter vs summer. *Canadian Journal of Fisheries and Aquatic Sciences Suppl.* (submitted).

Loder J. W. and D. G. Wright (1985) Tidal rectification and frontal circulation on the sides of Georges Bank. *Journal of Marine Research*, **43**, 581–604.

Lough R. G., W. G. Smith, F. E. Werner, J. W. Loder, F. H. Page, C. G. Hannah, C. E. Naimie, R. I. Perry, M. M. Sinclair and D. R. Lynch (1994) The influence of wind-driven advection on the interannual variability in cod egg and larval distributions on Georges Bank: 1982 vs 1985. *ICES Mar. Sci. Symp.*, **198**, 356–378.

Luettich R. A. Jr, S. Hu and J. J. Westerink (1994) Development of the direct stress solution technique for three-dimensional hydrodynamic models using finite elements. *International Journal for Numerical Methods in Fluids*, **19**, 295–319.

Luettich R. A. Jr and J. J. Westerink (1991) A solution for the vertical variation of stress, rather than velocity, in a 3-dimensional circulation model. *International Journal for Numerical Methods in Fluids*, **12**, 911–928.

Luettich R. A. and J. J. Westerink (1995) Continental shelf scale convergence studies with a barotropic tidal model. In: *Quantitative Skill Assessment for Coastal Ocean Models*, D. R. Lynch and A. M. Davies, editors, Coastal and Estuarine Series **48**, American Geophysical Union, Washington DC.

Luettich R. A. Jr, J. J. Westerink and N. W. Scheffner (1992) ADCIRC: an advanced three-dimensional circulation model for shelves coasts and estuaries, Report 1: theory and methodology of ADCIRD–2DDI and ADCIRC-3DL. *Dredging Research Program Technical Report DRP-92-6*, U.S. Army Engineers Waterways Experiment Station, Vicksburg, MS.

Lynch D. R. (1983) Progress in hydrodynamic modeling. Review of U.S. Contributions, 1979–1982. In: *Reviews of Geophysics and Space Physics*, **21**, 741–754.

Lynch D. R. and W. R. Gray (1979) A wave equation model for finite element computations. *Computers and Fluids*, **7**, 207–228.

Lynch D. R., J. T. C. Ip, C. E. Naimie and F. E. Werner (1995) Convergence studies of tidally-rectified circulation on Georges Bank. In: *Quantitative skill assessment for coastal ocean models*, D. R. Lynch and A. M. Davies, editors, Coastal and Estuarine Series **47**, American Geophysical Union, Washington, DC.

Lynch D. R. and C. E. Naimie (1993) The M2 tide and its residual on the outer banks of the Gulf of Maine. *Journal of Physical Oceanography*, **23**, 2222–2253.

Lynch D. R. and F. E. Werner (1987) Three-dimensional hydrodynamics on finite elements. Part I: linearized harmonic model. *International Journal for Numerical Methods in Fluids*, **7**, 871–909.

Lynch D. R. and F. E. Werner (1991a) Three-dimensional hydrodynamics on finite elements. Part II: non-linear time-stepping model. *International Journal for Numerical Methods in Fluids*, **12**, 507–533.

Lynch D. R. and F. E. Werner (1991b) Three-dimensional velocities from a finite element model of English Channel/southern bight tides. *Tidal Hydrodynamics*, B. Parker, editor, Wiley, NY, pp. 183–200.

Lynch D. R., F. E. Werner, A. Cantos-Figuerola and G. Parrilla (1989) Finite element modeling of reduced-gravity flow in the Alborán Sea: sensitivity studies. In: *Conferencia sobre oceanografía física del Estrecho de Gibraltar*, 24–28 October 1988, Madrid, J. L. Almazán *et al.*, editors, 283–295.

Lynch D. R., F. E. Werner, D. A. Greenberg and J. W. Loder (1992) Diagnostic model for baroclinic and wind-driven circulation in shallow seas. *Continental Shelf Research*, **12**, 37–64.

Lynch D. R., F. E. Werner, J. M. Molines and M. Fornerino (1990) Tidal dynamics in a coupled ocean/lake system. *Estuarine, Coastal and Shelf Science*, **31**, 319–343.

Ma H. (1993) A spectral element basin model for the shallow water equations. *Journal of Comput. Physics*, **109**, 133–149.

Mellor G. L. and T. Yamada (1982) Development of a turbulence closure model for geophysical fluid problems. *Reviews of Geophysics Space Physics*, **20**, 851–875.

Myers P. G. and A. J. Weaver (1995) A diagnostic barotropic finite-element ocean circulation model. *Journal of Atmospheric and Oceanic Technology* (in press).

Naimie C. E. (1995) On the modeling of the seasonal variation of the three-dimensional circulation near Georges Bank. Ph.D. thesis, Dartmouth College, Hanover, New Hampshire.

Naimie C. E., J. W. Loder and D. R. Lynch (1994) Seasonal variation of the 3-D residual circulation on Georges Bank. *Journal of Geophysical Research*, **99** (C8), 15967–15989.

Naimie C. E. and D. R. Lynch (1993) Three-dimensional diagnostic model for baroclinic, wind-driven and tidal circulation in shallow seas—FUNDY5 users' manual. Numerical Methods Laboratory Report NML-93-1, Dartmouth College, Hanover, New Hampshire, March 1993.

Pearson C. E. and D. F. Winter (1977) On the calculation of tidal currents in homogeneous estuaries. *Journal of Physical Oceanography*, **7**, 520–531.

Pettigrew N. R. (1994) The observational basis for subtidal circulation in the Gulf of Maine. Gulf of Maine circulation modeling: workshop proceedings, E. Braasch, editor, Regional Association for Research on the Gulf of Maine, Report No. 94–1, Dartmouth College, Hanover, NH, pp. 3–19.

Pinder G. F. and W. G. Gray (1977) *Finite element simulation in surface and subsurface hydrology*, Academic Press, 295 pp.

Platzman G. W. (1978) Normal modes of the world ocean. Part I. Design of a finite element barotropic model. *Journal of Physical Oceanography*, **8**, 323–343.

Praagman N., J. Dijkzeul, R. van Dijk and R. Pleiger (1989) A finite difference simulation model for tidal flow in the English Channel and southern North Sea. *Advances in Water Resources*, **12**, 155–164.

Price J. F. (1979) On the scaling of stress driven entrainment experiments. *Journal of Fluid Mechanics*, **90**, 509–529.

Ridderinkhof H. and J. W. Loder (1994) Lagrangian characterization of circulation over submarine banks with application to the outer Gulf of Maine. *Journal of Physical Oceanography*, **24**, 1184–1200.

RMRP (1992) *Gulf of Maine research plan*. Gulf of Maine Regional Marine Research Program, University of Maine, June 1992.

Smagorinsky J. (1963) General circulation experiments with the primitive equations I. The basic experiment. *Monthly Weather Review*, **91**, 99–164.

Tee K.-T., P. C. Smith and D. LeFaivre (1993) Topographic upwelling off southwest Nova Scotia. *Journal of Physical Oceanography*, **23**, 1703–1726.

Townsend D. W. (1989) The implications of slope water intrusions in the Gulf of Maine. Proceedings of a Workshop, 6–7 March 1989, D. W. Townsend, editor, sponsored by ARGO-Maine, Bigelow Laboratory for Ocean Sciences.

Tremblay M. J., J. W. Loder, F. E. Werner, C. E. Naimie, F. H. Page and M. M. Sinclair (1994) Drift of sea scallop larvae *Placopecten magellanicus* on Georges Bank: a model study of the roles of mean advection, larval behavior and larval origin. *Deep Sea Research II*, **41** (1), 7–49.

Vincent P. and C. Le Provest (1988) Semi-diurnal tides in the north-east Atlantic from a finite element numerical model. *Journal of Geophysical Research*, **93**, 543–555.

Wang J. D. and J. J. Connor (1975) Mathematical modeling of near coastal circulation. Technical Report No. 200, Ralph M. Parsons Laboratory, MIT, Cambridge, MA.

Walters R. A. (1987) A model for tides and currents in the English Channel and southern North Sea. *Advances in Water Resources*, **10**, 138–148.

Walters R. A. (1992) A three-dimensional, finite element model for coastal and estuarine circulation. *Continental Shelf Research*, **12**, 83–102.

Walters R. A. and G. F. Carey (1984) Numerical noise in ocean and estuarine models. *Advances in Water Resources*, **7**, 15–20.

Walters R. A. and M. G. G. Foreman (1992) A 3D, finite element model for baroclinic circulation on the Vancouver Island continental shelf. *Journal of Marine Systems*, **3**, 507–518.

Walters R. A. and F. E. Werner (1989) A comparison of two finite element models using the North Sea data set. *Advances in Water Resources*, **12**, 184–193.

Werner F. E. (1987) A numerical study of secondary flows over continental shelf edges. *Continental Shelf Research*, **7**, 379–409.

Werner F. E. (1995) A field test case for tidally forced flows: a review of the tidal flow forum. In: *Quantitative skill assessment for coastal ocean models*, D. R. Lynch and A. M. Davies, editors, Coastal and Estuarine Series **47**, American Geophysical Union, Washington, DC.

Werner F. E., J. O. Blanton, D. R. Lynch and D. K. Savidge (1993a) A numerical study of the continental shelf circulation of U.S. South Atlantic Bight during autumn of 1987. *Continental Shelf Research*, **13**, 971–997.

Werner F. E. and D. R. Lynch (1987) Field verification of wave equation tidal dynamics in the English Channel and southern North Sea. *Advances in Water Resources*, **10**, 115–130.

Werner F. E. and D. R. Lynch (1988) Meeting report: 2nd tidal flow forum. *EOS*, **69**, 1027–1028.

Werner F. E. and D. R. Lynch (1989) Harmonic structure of English Channel/southern Bight tides from a wave equation simulation. *Advances in Water Resources*, **12**, 121–142.

Werner F. E., F. H. Page, D. R. Lynch, J. W. Loder, R. G. Lough, R. I. Perry, D. A. Greenberg and M. M. Sinclair (1993b) Influences of mean advection and simple behavior on the distribution of cod and haddock early life stages on Georges Bank. *Fisheries Oceanography*, **2**, 43–64.

Westerink J. J., R. A. Luettich Jr, A. M. Baptista, N. W. Scheffner and P. Farrar (1992) Tide and storm surge predictions using a finite element model. *ASCE Journal of Hydraulic Engineering*, **118**, 1373–1390.

Westerink J. J., R. A. Luettich Jr and J. Muccino (1994) Modeling tides in the western North Atlantic using unstructured graded grids. *Tellus*, **46A**, 178–199.

Westerink J. J., K. D. Stolzenbach and J. J. Connor (1989) General spectral computations of the nonlinear shallow water tidal interactions within the Bight of Abaco. *Journal of Physical Oceanography*, **19**, 1348–1371.

Wiggin J. and C. N. K. Mooers (1992) Proceedings of the Gulf of Maine Scientific Workshop, Urban Harbors Institute, U. Mass., Boston, December 1992.

Woodruff S. D., R. J. Slutz, R. L. Jenne and P. M. Steurer (1987) A comprehensive ocean-atmosphere data set. *Bulletin of the American Meteorological Society*, **68**, 1239–1250.

Wright D. G. and K. R. Thompson (1983) Time-averaged forms of the nonlinear stress law. *Journal of Physical Oceanography*, **13**, 341–345.